Reward Engineering for Spatial Epidemic Simulations: A Reinforcement Learning Platform for Individual Behavioral Learning

Anonymous authors
Paper under double-blind review

Abstract

We present ContagionRL, a Gymnasium-compatible reinforcement learning platform specifically designed for systematic reward engineering in spatial epidemic simulations. Unlike traditional agent-based models that rely on fixed behavioral rules, our platform enables rigorous evaluation of how reward function design affects learned survival strategies across diverse epidemic scenarios. ContagionRL integrates a spatial SIRS+D epidemiological model with configurable environmental parameters, allowing researchers to stress-test reward functions under varying conditions including limited observability, different movement patterns, and heterogeneous population dynamics. We evaluate five distinct reward designs, ranging from sparse survival bonuses to a novel potential field approach, across multiple RL algorithms (PPO, SAC, A2C). Through systematic ablation studies, we identify that directional guidance and explicit adherence incentives are critical components for robust policy learning. Our comprehensive evaluation across varying infection rates, grid sizes, visibility constraints, and movement patterns reveals that reward function choice dramatically impacts agent behavior and survival outcomes. Agents trained with our potential field reward consistently achieve superior performance, learning maximal adherence to non-pharmaceutical interventions while developing sophisticated spatial avoidance strategies. The platform's modular design enables systematic exploration of reward-behavior relationships, addressing a knowledge gap in models of this type where reward engineering has received limited attention. ContagionRL is an effective platform for studying adaptive behavioral responses in epidemic contexts and highlight the importance of reward design, information structure, and environmental predictability in learning.

1 Introduction

The dynamics of infectious outbreaks, epidemics or pandemics, are intricately linked to individual behavior (Wang et al., 2021; Funk et al., 2010). Behavioral decisions such as movements, risk perceptions and adherence to non-pharmaceutical interventions (such as mask-wearing and social distancing) could heavily affect how an epidemic unfolds (Wang et al., 2021; Funk et al., 2010; Manrubia & Zanette, 2022; Ye et al., 2020; Saad-Roy & Traulsen, 2023). Traditional epidemic models primarily use ordinary differential equations (ODEs) to keep track of disease population-wide with models such as SIR (Kermack & McKendrick, 1927) or SEIR (Kermack & McKendrick, 1927; Wilson & Worcester, 1945). While these models are effective for a high-level overview of the disease outbreak, due to their assumption of homogeneity, they neglect nuanced effects of individual behavior and spatial interactions (Bansal et al., 2007; Zachreson et al., 2022). Furthermore, they are incapable of capturing dynamic behavioral changes or adaptive interventions (Funk et al., 2010; Manrubia & Zanette, 2022; Bansal et al., 2007).

The SARS-CoV-2 pandemic highlighted how individual-level decisions and behaviors, such as adherence to non-pharmaceutical interventions (NPIs) like mask wearing, could profoundly change the trajectory of a disease outbreak (Saad-Roy & Traulsen, 2023). Agent-Based Models (ABMs) (Grimm & Railsback, 2013), also known as Individual-Based Models (IBMs), offer a compelling alternative by simulating systems from the bottom up, representing individual agents with specific attributes, spatial contexts, and behavioral rules. These models accommodate heterogeneity and complex interactions, thereby making ABMs particularly suitable for studying epidemics where individual actions drive epidemic-scale outcomes, while leaving them reliant on prescribed or rule-based behaviors rather than learned policies that exhibit more complexity and are more dynamic (Grimm & Railsback, 2013).

The lack of the learned policies could be addressed with Reinforcement Learning (RL) (Sutton & Barto, 2018) and Deep Reinforcement Learning (DRL) (Li, 2017; Mousavi et al., 2016; François-Lavet et al., 2018) that provide powerful frameworks to optimize sequential decision making in dynamic systems (Mnih et al., 2015; Silver et al., 2016; Arulkumaran et al., 2017) by modeling them as Markovian decision processes (MDP). Such algorithms have been applied in epidemiological contexts to learn the optimal policies by focusing on centralized control of macroscopic interventions (Libin et al., 2021; Kwak et al., 2021; Du et al., 2023; Wan et al., 2021). Combining of RL or DRL algorithms with ABMs allows simulation of both adaptive and heterogeneous behaviors.

However, the main challenge in creating and developing informative ABMs lies in defining realistic and computationally tractable agent behaviors. Furthermore, RL-based approaches are highly sensitive to the reward function and the reward design can have considerable impact on the learned policy and the downstream interpretations of the model upon behavioral convergence (Ng et al., 1999; Ibrahim et al., 2024; Nguyen et al., 2025; Shihab et al., 2025).

Currently, there are limited simulation platforms capable of supporting the integration of RL that permit the agents to learn complex strategies for navigation and adherence strategies by direct interaction within their environment. This creates an important gap in the tools for investigating impact of reward design on learned dynamic behaviors at the individual level within biologically sound epidemic simulations.

To address this, we introduce ContagionRL, a specialized reinforcement learning platform designed to study how different reward structures influence agent behavior during epidemic simulations. This is a novel and parameterizable, Gymnasium compatible environment that unifies spatial compartmental epidemic modeling and reinforcement learning. We integrate an extension of a Susceptible-Infected-Recovered-Susceptible (SIRS) framework called SIRS+D, which has an additional component for death, to track population-wide epidemiological dynamics, while also enabling the use of RL to model individual-level decision-making. This environment simulates a single learning agent among a population of non-learning humans, whose movements affect the disease outbreak. In this setting, we frame the agent's decision making as a sequential control problem in which the agent learns behavioral policies through direct interaction with the environment. These policies include both spatial navigation and adherence to non-pharmaceutical interventions (NPIs), developed in response to localized epidemic conditions. Table 3 compares our models to other approaches.

To demonstrate the effectiveness of this novel environment, we conduct a variety of experiments. We investigate the nature of the policies learned by this RL agent under varying epidemiological and behavioral conditions. In addition, we conduct ablation studies to understand the critical components of the reward function that is the most impactful in the learning process. Benchmarking shows that these learned policies significantly outperform random and stationary baselines in terms of survival time. An ablation study shows the importance of both directional cues and adherence incentives within the reward function to learn a robust, risk-averse behavior. Across all effective reward structures, the agent consistently learned maximal adherence to NPIs. This framework provides a modular and highly configurable environment for studying emergent behaviors at the individual level within spatial epidemic models.

2 Related Works

Compartmental Models in Epidemiology. Classical epidemiological models, such as SIR (Susceptible-Infected-Recovered), divide a population into discrete groups (compartments) based on disease state (Kermack & McKendrick, 1927; Wilson & Worcester, 1945). The flow of individuals between compartments is described by ordinary differential equations (ODEs). Extensions like SEIR (adding an exposed group to act as a disease incubation period) or SVE(R)IRS (adding Vaccinated, accounting for waning immunity) incorporate more states to increase realism (Brauer et al., 2019; Friedman & Kao, 2014; Hethcote, 2000; Chyba et al., 2024;

Balisacan et al., 2021). While traditional compartmental models provide valuable population-level insights, assumptions of homogeneity limit their ability to represent individual decision-making (Cangiotti et al., 2024; Siegenfeld et al., 2022; Dimarco et al., 2021; Jiang et al., 2024; Bostanci & Conrad, 2025; Rose et al., 2021; Kong et al., 2016). These models also struggle to capture dynamic behavioral changes or adaptive interventions (Brauer et al., 2019; Siegenfeld et al., 2022). Ignoring such factors can limit accuracy and lead to misleading conclusions (Sudhakar et al., 2024; Siegenfeld et al., 2022). Stochastic formulations are particularly relevant for small populations or during the early stages of an outbreak (Brauer et al., 2019).

Agent-Based Models (ABMs). ABMs address the limitations of compartmental models like SIR by modeling heterogeneous individuals using specific attributes and interaction rules within an environment or network (Tracy et al., 2018; Hunter et al., 2018; 2017). Furthermore, ABMs excel at capturing individual variability, stochasticity, local interactions, and complex contact networks, which are difficult for compartmental models (Siegenfeld et al., 2022; Hunter et al., 2017). Recent advances demonstrate substantial sophistication such as large-scale ABMs that can simulate millions of agents with GPU acceleration (Chopra et al., 2021) or employ LLM-based adaptive agents (Park et al., 2023).

Challenge of Reward Engineering. Sophisticated ABMs show potential for learning-enabled epidemic modeling. However, systematic evaluation of reward function design remains an important methodological gap. In reinforcement learning, reward design shapes the fundamentals of the learned behavior with different reward structures leading to considerably different learned policies at convergence (Ng et al., 1999; Amodei et al., 2016; Nguyen et al., 2025; Shihab et al., 2025). Despite the importance of this problem in RL, epidemic modeling applications have not systematically investigated how reward structure affects learning under varying conditions.

Reinforcement Learning (RL) for Epidemics. RL has been increasingly leveraged to design policies for epidemic intervention at population and individual level. Individual-based Reinforcement Learning Epidemic Control Agent (IDRLECA) proposed an RL agent at an individual level using GNNs to estimate infection probabilities and balance epidemic suppression vs cost of mobility in its reward function (Feng et al., 2023). VEHICLE (Feng et al., 2022) handles challenges of unobservable asymptomatic cases and delayed effects by using a combination of hierarchical RL with GNNs. Recent work has also focused on using actor critic methods to minimize a cost that considers both the epidemiological, economic and social cost for multi-intervention planning (Mai et al., 2023) or using RL for scheduling lockdown periods (Arango & Pelov, 2020) that incorporates the ICU capacity and minimizing time spent in lockdowns. HRL4EC (Du et al., 2023) also leverages hierarchical RL and multi-component reward that considers both health and socioeconomic cost. SiRL (Bushaj et al., 2023) uses a detailed ABM with RL and feeds the compartmental levels to the agent and uses rewards that are tied to intervention effectiveness and disease spread. These approaches excel at macro-level policy optimization such as determining lockdown time, resource allocation, and intervention sequencing (Mai et al., 2023; Arango & Pelov, 2020; Khadilkar et al., 2020). While valuable for analyzing epidemic policy, these centralized approaches do not examine the impact of different reward formulations on the learned RL policy.

Addressing the Reward Engineering Gap. This work addresses this gap by providing a systematic framework for evaluating reward formulation in spatial epidemic simulations. Instead of assuming particular behavioral patterns, we investigate the impact of different reward structure, varying environmental conditions such as partial observability, different infection rates, population density, distance decay factor (strength of disease transmission over distance), effectiveness of adherence to non-pharmaceutical interventions and spatial constraints, on learned behavior.

3 Methodology

ContagionRL is a custom Gymnasium-compatible (Towers et al., 2024) environment that integrates a SIRS+D compartmental epidemiological model (Hethcote, 2000). Built within an agent-based modeling framework, the environment simulates a single reinforcement learning (Sutton & Barto, 2018) agent interacting with a population of humans whose behaviors may be stochastic or deterministic or mix of both. This design enables the study of learned risk-averse navigation and adherence behaviors in response to an evolving epidemic (Saad-Roy & Traulsen, 2023) in different contexts.

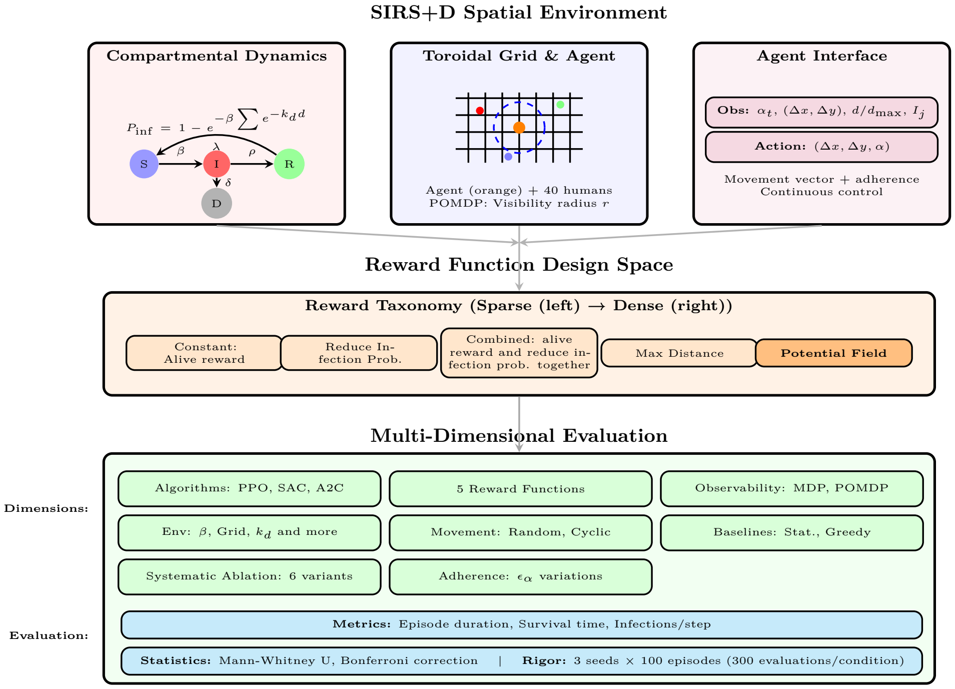
SIRS+D Spatial Environment
Compartmental Dynamics
$P_{\text{inf}} = 1 - e^{-\beta \sum e^{-k_d d}}$
S
I
R
D
β
λ
ρ
δ
Toroidal Grid & Agent
Agent (orange) + 40 humans
POMDP: Visibility radius r
Agent Interface
Obs: α_t, $(\Delta x, \Delta y)$, $d/d_{\max}$, I_j
Action: $(\Delta x, \Delta y, \alpha)$
Movement vector + adherence
Continuous control
Reward Function Design Space
Reward Taxonomy (Sparse (left) → Dense (right))
Constant: Alive reward
Reduce Infection Prob.
Combined: alive reward and reduce infection prob. together
Max Distance
Potential Field
Multi-Dimensional Evaluation
Dimensions:
Algorithms: PPO, SAC, A2C
5 Reward Functions
Observability: MDP, POMDP
Env: β, Grid, k_d and more
Movement: Random, Cyclic
Baselines: Stat., Greedy
Systematic Ablation: 6 variants
Adherence: ϵ_α variations
Evaluation:
Metrics: Episode duration, Survival time, Infections/step
Statistics: Mann-Whitney U, Bonferroni correction | Rigor: 3 seeds × 100 episodes (300 evaluations/condition)

Figure 1: **ContagionRL System Architecture. Top:** SIRS+D spatial epidemic environment with toroidal grid, configurable observability, and continuous agent control interface. **Middle:** Reward function design from sparse to potential field-based rewards. **Bottom:** Multi-dimensional experimental evaluation.

Single Agent Design Rationale. Epidemic dynamics are inherently multi-agent interactions (Manfredi & D'Onofrio, 2013; Wang et al., 2016). However, our single agent approach is a methodological choice that enables us to evaluate the design of the reward function in a systematic format. Multi-agent environments introduce complexities such as non-stationarity due to other learning agents (Foerster et al., 2017), emergent social behavior (Leibo et al., 2017) and strategic interactions (Tampuu et al., 2017). Each of these complexities can complicate and potentially obfuscate how specific reward components influence the learned policy at an individual level. The isolation of the learning process to a single agent in a controlled population of non-learning humans, allows for transparent study of the impact of reward structure. This permits the identification of essential reward components for effective behavior learning. Furthermore, this presents a first step for understanding the relationship between reward and behavior before applying insights to a complex domain like multi-agent reinforcement learning. By isolating a single learning agent, in a controlled population of non-learning humans, we can conduct detailed assessments of how different reward formulations affect the learned strategies without interference from adaptive social behaviors. The controlled nature of this methodology allows insights into the relationship between reward and behavior, that will be transferable to more complex multi-agent deployments where understanding individual level incentive responses becomes critical for designing effective reward systems across a population.

3.1 SIRS+D Simulation Environment

Environment Dynamics. The simulation happens over discrete timesteps within a two-dimensional grid space of size $G \times G$ with periodic boundary conditions (Allen et al., 2009; Keeling & Rohani, 2008; Frenkel & Smit, 2002). The environment is populated by N non-learning humans and a single controllable Reinforcement Learning (RL) agent. Each individual, human or agent, can exist in one of four states: Susceptible (S), Infected (I), Recovered (R), or Dead (D). We conduct a set of sensitivity analysis in Appendix F and vary the infection rate of disease (β) in Figure 12 and Table 11, vary the grid size and population density in Figure 13 and Table 12, vary the adherence effectiveness (α_{eff}) in Figure 14 and Table 13, and vary the distance decay of disease transmission in Figure 15 and Table 14.

Human Movement and State Transitions. Non-learning humans exhibit stochastic or deterministic movement based on a specified movement type with a defined movement scale. Stochastic humans make their decisions by sampling from a Gaussian distribution within the bounds of the action space used to mimic the noisy nature of observation perception by the learning RL agent. Conversely, the deterministic non-learning humans are used to mimic the social and spatial constraints of a pandemic such as commuting. Their state transitions are governed by probabilistic rules. A susceptible human h_s becomes infected with a probability $P_{\text{inf}}(h_s)$, determined by their exposure to nearby infected individuals h_i. Exposure is calculated based on the distance $d(h_s, h_i)$ between the susceptible human and each infected human, potentially limited by a maximum distance. The infection probability follows $P_{\text{inf}}(h_s) = 1 - \exp(-\beta \sum_{h_i} e^{-k_d \cdot d(h_s, h_i)})$, where β is the base infection rate and k_d is the distance decay factor. Once infected, a human recovers with a fixed probability ρ at each timestep. After recovery, a human may lose immunity and revert to the susceptible state with a probability λ at each timestep. Infected humans may also die with a probability δ at each timestep. Dead humans are removed from contributing to infection spread and cease movement. Appendix C.2 contains a description of environmental parameters and their descriptions.

Agent Dynamics and Control. The agent operates under SIRS+D dynamics identical to other individuals but differs in that it actively selects its movement and adherence levels via a learned policy. These choices affect both its spatial trajectory and susceptibility to infection. For a detailed formalization of the agent's action space, including adherence effects and boundary handling, see Section 3.2. Figure 8 shows a render of the environment.

Initialization and Episode Structure. Each simulation run begins with the agent positioned on the grid's center. The non-agent humans are distributed randomly, with an parameterization number of individuals set to the infectious (I) state. These initial infectees are placed at least a minimum safe distance from each other and from the agent. All remaining humans commence in the 'S' state, ensuring a minimum initial distance from the agent's starting position. The minimum safe distances are used to prevent trivial early termination of a simulation. The agent itself always starts as Susceptible ('S') with a predefined initial adherence level. To counteract stochastic extinction of the disease and trivial success episodes, a configurable reinfection mechanism is employed. If the number of infected individuals reaches zero, a specified number of susceptible humans (located beyond the minimum safe distance from the agent) are randomly chosen and transitioned back to the 'I' state. An episode concludes upon reaching the maximum simulation time limit. Termination can occur early if the agent transitions to infected ('I' state), or if the infection is eradicated and the reinfection mechanism cannot be activated due to insufficient eligible susceptible individuals.

3.2 RL Agent Formulation

We implement the agent's learning problem as a configurable decision-making process that supports both Markov Decision Process (MDP) and Partially Observable MDP (POMDP) formulations. We use both the MDP and POMDP formulation in our experiments. The POMDP employs a threshold-based visibility constraint, where agents can only observe other entities within a specified Euclidean distance radius. The agent's policy $\pi(a_t|o_t)$, mapping observations to actions, is learned using three deep reinforcement learning algorithms: Proximal Policy Optimization (PPO) (Schulman et al., 2017), Soft Actor-Critic (SAC) (Haarnoja et al., 2018), and Advantage Actor Critic (A2C) a synchronous variant of A3C algorithm (Mnih et al., 2016), all implemented via the STABLE-BASELINES3 library (Raffin et al., 2021).

Observation Space. The observation space provides the agent with information about its internal state and the surrounding environment at each timestep t. The observation o_t, constructed via the environment's internal observation method, is comprising the agent's current adherence level α_t (a scalar in $[0, 1]$) and a flattened feature vector describing the non-learning population. This vector aggregates information for each non-learning human h_j. For every human h_j, the features consist of the relative position $(\Delta x_{aj}, \Delta y_{aj})$, representing the normalized displacement from the agent calculated considering toroidal boundaries and scaled by grid size (values in $[-0.5, 0.5]$); the normalized distance $(d_{aj}/d_{\max})$, which is the Euclidean distance scaled by the maximum possible grid diagonal distance $d_{\max}$; and a binary infection status indicator (I_j).

Action Space. At each timestep t, the agent selects a continuous-valued action $a_t = (\Delta x, \Delta y, \alpha)$, where $(\Delta x, \Delta y) \in [-1, 1]^2$ defines a movement vector and $\alpha \in [0, 1]$ specifies the adherence level to non-pharmaceutical interventions (NPIs). NPIs are methods used to reduce the spread of an epidemic disease without any pharmaceutical drug treatments such as wearing masks or social distancing and are considered extremely effective ways of controlling primary outbreaks that reduce disease transmission and consequentially mortality (Rizvi et al., 2021; Ferguson et al., 2020). The agent's position is updated using the movement vector, scaled by a maximum step size, and wrapped around the grid's periodic boundaries:

$$x_{t+1} = (x_t + \Delta x) \bmod G, \quad y_{t+1} = (y_t + \Delta y) \bmod G, \tag{1}$$

where G is the grid size. The adherence level α directly influences the agent's probability of infection upon exposure to nearby infected individuals by modulating the effective infection rate:

$$\beta_{\text{eff}} = \beta \cdot (\epsilon_\alpha + (1 - \epsilon_\alpha)(1 - \alpha)) \tag{2}$$

where $\epsilon_\alpha \in (0, 1)$ represents the residual infection risk at full adherence. Thus, higher adherence values reduce susceptibility, but never eliminate risk entirely.

3.3 Reward Functions

To investigate the impact of reward engineering on policy learning within the ContagionRL environment, we implemented and evaluated several distinct reward functions. These functions vary in complexity and the specific agent behaviors they aim to incentivize, with the overarching goal of prolonging the agent's susceptible state. The simplest among these is a Constant Reward, which provides a fixed positive signal if the agent remains uninfected. The Reduce Infection Probability reward directly incentivizes the agent to minimize its calculated likelihood of infection at each step, based on exposure to nearby infected individuals and its current adherence level. This can be employed as a Combined Reward by supplementing it with the constant bonus. Another approach, Maximize Nearest Distance, focuses on spatial dynamics, rewarding the agent for maintaining a distance from the closest susceptible or infected individuals, particularly beyond a predefined threshold.

The most complex of the explored designs is the Potential Field Reward. This function models interactions as forces, where other agents (particularly infected ones) exert repulsive forces on the agent. The reward encourages movement that aligns with the net resultant force vector, effectively guiding the agent away from high-risk areas. This directional guidance is complemented by terms rewarding the agent for its health status and NPI adherence. These reward function are tested in different environmental configuration. Details of the reward calculation are provided in Appendix C.3.

4 Baselines

To contextualize the performance of the learned policies with RL, we established several non-learning deterministic baselines. These policies represent simple, fixed strategies and serve as benchmarks to evaluate the complexity and effectiveness of the learned behavior. We implemented three distinct baseline strategies (see Appendix C.5 for more details).

Stationary Baseline. This agent remains immobile with zero adherence to NPIs ($\Delta x = \Delta y = \alpha = 0$) throughout the episode. Its performance depends entirely on initial conditions and the stochastic behavior of the surrounding population.

Random Baseline. At each timestep, this agent samples movements $\Delta x, \Delta y \sim \mathcal{U}(-1, 1)$ and adherence $\alpha \sim \mathcal{U}(0, 1)$, while being oblivious with regard to the environment and observations entirely. It serves as a reference for performance under uninformed, mobile behavior.

Greedy Distance Maximizer Baseline. This heuristic policy implements a specific survival strategy focused on immediate risk avoidance. At each step, it first identifies the nearest infected human. It then evaluates a predefined set of potential movement actions across the eight cardinal and intercardinal directions, plus staying stationary. It systematically simulates the outcome of a each potential action, by computing the hypothetical distance to the nearest infected human if that move were taken, and selects the action that yields the greatest distance separation. The policy's evaluation of counterfactual outcomes provides a situational awareness absent in simpler baselines. While myopic and handcrafted, this policy provides a strong heuristic benchmark by explicitly evaluating the spatial consequence of each potential action.

5 Results

Performance of different algorithms in ContagionRL environment. To evaluate the utility of the ContagionRL for obtaining effective learned policies via reinforcement learning (RL), we trained and assessed three distinct RL algorithms: Soft Actor-Critic (SAC) (Schulman et al., 2017), Proximal Policy Optimization (PPO) (Schulman et al., 2017), and Advantage Actor-Critic (A2C) (Mnih et al., 2016). Their performance was benchmarked against baselines mentioned in section 4 (configuration details are in Appendix C.2 and Appendix C.4).

Figure 2 shows the distribution of episode durations for both baselines and the RL agents. The distributions of episode duration for the stationary and random baselines have substantially less variance compared to those of the RL agents and the greedy heuristic. To determine the statistical significance of these different distributions, we conducted pairwise comparisons using the Mann-Whitney U test. The outcomes of these tests, including both two-sided and one-sided p-values, are presented in Table 1.

The statistical analyses reveal that the learned policies derived from the RL approaches (PPO, SAC, and A2C) significantly outperform both the random and stationary baselines. The greedy heuristic baseline demonstrates superior performance in pairwise comparisons against all three RL agents, achieving statistically significantly longer episode durations (Table 1). However, as depicted by the mean episode durations and their 95% confidence intervals in Figure 9, the performance of the RL agents is comparable to that of the greedy baseline, with overlapping confidence intervals.

This tells us that while the distributions of episode durations and their medians, differ significantly in favor of the greedy approach, the mean performance of greedy does not outperform learned RL policies. These results collectively demonstrate several key points: (1) The observation formulation within the ContagionRL environment provides a sufficient and informative signal for the RL agents to develop effective control policies that substantially exceed naive baselines. (2) The environment supports the application and comparative evaluation of various RL algorithms, highlighting their compatibility with its inherent stochasticity and complex dynamics, leading to policies competitive with a strong heuristic. (3) While a specialized greedy heuristic can achieve statistically superior median performance, the learned RL agents develop sophisticated strategies that yield comparable mean performance, showing the environment's utility for investigating adaptive decision-making processes that can approach the efficacy of well-designed heuristics without explicit rule-based programming used in ABMs.

Comparison of Different Reward functions in ContagionRL. Our primary algorithm evaluations utilized a potential field-based reward. Now, we investigate the differential impact of diverse reward structures on performance. We use the environment configuration in Appendix C.2 and alter the reward functions to gauge difference in performance with PPO. The principal objective for the agent remains the avoidance of infection. This is quantified by the episode duration, which measures the number of timesteps during which the agent remains susceptible before experiencing its first infection. In other words, if the agent becomes infected for the first time at timestep t, the achieved episode duration is $t - 1$. Although alternative reward schemes could be designed to elicit and study different behaviors, our focus here is on optimizing for this primary goal.

Figure 3 and Figure 10 visually summarize the performance distributions and mean episode durations, respectively, for policies trained under five distinct reward functions (see Section 3.3 and Appendix C.3). The statistical significance of these differences is further detailed in Table 8, which presents pairwise Mann-Whitney U test comparisons against the Potential Field baseline.

The results indicate that the Potential Field reward function, via its dense and spatially informed feedback, results in a significantly superior performance, achieving the longest mean episode durations. Policies trained with the Constant reward structure show poor performance. We attribute this to the sparse and uninformative nature of a constant bonus, which provides little guidance for nuanced decision-making. Similarly, the Max

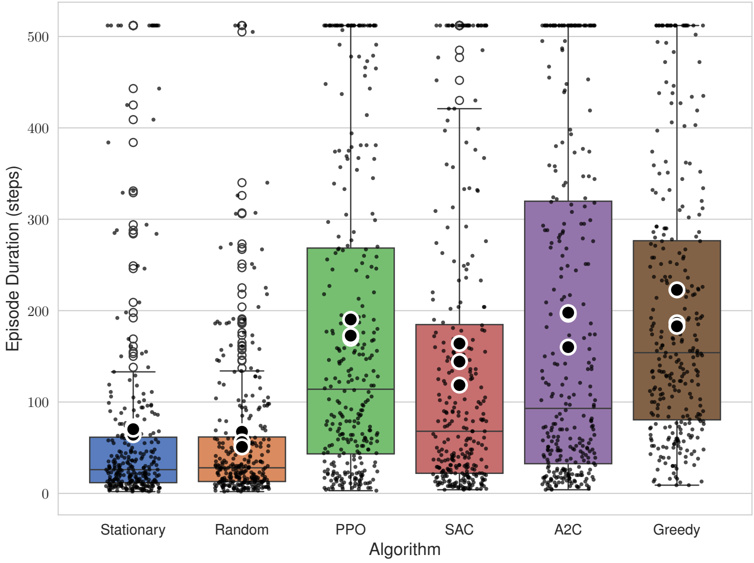

Figure 2: Episode duration distributions across different agents, including learning-based (PPO, SAC, A2C) and non-learning baselines (Random, Stationary, Greedy). Each small black dot represents one episode in the totality of episodes across 3 seeds × 100 evaluation runs. Per-seed means are shown as large black dots with white outlines. This figure complements the summary statistics in Figure 9 and statistical comparisons in Table 1.

Table 1: Pairwise comparisons of episode durations between agents using the Mann–Whitney U test. Two-sided p-values assess distributional differences, and one-sided p-values (Bonferroni-corrected) test for performance advantage. The **Winner** is the agent with significantly longer episode duration (after correction); "–" indicates no significant difference. Significance codes: * $p < 0.05$, ** $p < 0.01$, *** $p < 0.001$, n.s. = not significant.

Agent A	**Agent B**	**p (2-sided)**	**p (1-sided)**	**Sig (2)**	**Corrected p (1)**	**Sig (1)**	**Winner**
Stationary	Random	0.5594	0.7204	n.s.	1	n.s.	–
Stationary	PPO	3.22e-25	1.61e-25	***	2.42e-24	***	PPO
Stationary	SAC	3.83e-13	1.92e-13	***	2.88e-12	***	SAC
Stationary	A2C	2.46e-22	1.23e-22	***	1.84e-21	***	A2C
Stationary	Greedy	3.87e-48	1.94e-48	***	2.91e-47	***	Greedy
Random	PPO	1.39e-25	6.96e-26	***	1.04e-24	***	PPO
Random	SAC	1.27e-12	6.32e-13	***	9.49e-12	***	SAC
Random	A2C	1.29e-22	6.45e-23	***	9.68e-22	***	A2C
Random	Greedy	9.96e-51	4.98e-51	***	7.47e-50	***	Greedy
PPO	SAC	0.00103	0.00052	**	0.00775	**	PPO
PPO	A2C	0.7604	0.62	n.s.	1	n.s.	–
PPO	Greedy	0.000639	0.000320	***	0.00479	**	Greedy
SAC	A2C	0.00430	0.00215	**	0.0323	*	A2C
SAC	Greedy	1.06e-12	5.28e-13	***	7.93e-12	***	Greedy
A2C	Greedy	0.000341	0.000171	***	0.00256	**	Greedy

Nearest Distance reward function also resulted in significantly shorter episode durations compared to the Potential Field approach.

Both the Max Nearest Distance and the Reduce Infection probability reward functions may guide the agent towards suboptimal local optimas. An agent might learn to maintain a specific distance from currently infected individuals, thereby maximizing its immediate reward. However, it fails to adopt a globally optimal positioning strategy that minimizes long-term infection risk. This highlights the challenge of designing reward functions that encourage far-sighted behavior rather than myopic optimization in complex spatial settings.

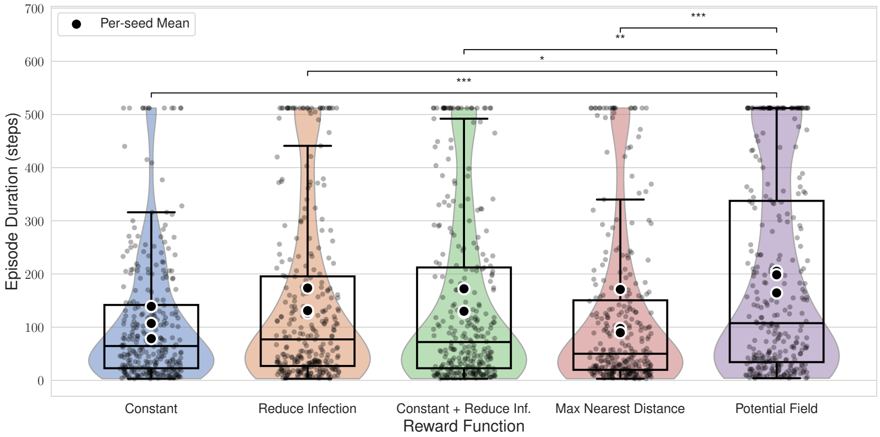

Figure 3: Comparison of PPO agent performance under five different reward functions. Each model was trained with three random seeds and evaluated over 100 episodes per seed (300 episodes total per reward function). Violin plots show the distribution of episode durations, overlaid with boxplots and per-episode results (black points). Large black dots with white outlines indicate the per-seed mean. One-sided Mann–Whitney U tests (with Bonferroni correction) compare each reward function to the *Potential Field* baseline. Statistically significant differences (* $p < 0.05$, ** $p < 0.01$, *** $p < 0.001$) are annotated. See Table 8 for exact test values and Figure 10 for corresponding means with confidence intervals.

An important observation, across all tested reward functions, is the consistent emergence of high NPI adherence in the learned policies. This suggests that the benefit of maximizing adherence is a relatively identifiable signal within the ContagionRL environment, discoverable through learning irrespective of the specific reward structure guiding navigation. The primary challenge lies in learning effective spatial navigation strategies, a task for which the choice of reward function is more important. The data presented in Figures 3 and 10, and substantiated by the statistical comparisons in Table 8, unequivocally demonstrate the influence of reward function design on the learned policy to achieve the desired infection avoidance behavior.

Ablations of reward function. To understand the contributions of individual components to the overall efficacy of the potential field reward function, we conduct a systematic ablation study. Specific elements of the full potential field (FPF) reward were individually removed, and the performance of policies trained with these ablated reward structures was compared against the FPF baseline. We use the same configuration as the previous section but changed the value of the reward ablation field (Appendix C.2). We did the following ablations: removal of the movement magnitude component (No Magnitude), removal of the directional component of movement (No Direction), removal of the entire movement-related reward (No Movement), removal of the adherence-based reward (No Adherence), removal of the health status reward (No Health), and removal of the repulsion force from susceptible individuals (No Susceptible Repulsion). The comparative performance distributions are illustrated in Figure 4, mean performances are shown in Figure 11, and detailed statistical comparisons are presented in Table 9.

The results (Table 9) indicate that several components are important to the FPF reward's success. Specifically, the removal of the directional guidance (No Direction), the overall movement incentive (No Movement), or the reward for NPI adherence (No Adherence) led to a statistically significant and substantial degradation in performance of learned policy compared to the FPF as our baseline. These elements provide the primary signal guiding the agent's navigation to safer regions. Without this explicit directional information, the agent's ability to learn effective spatial strategies is severely impaired.

The ablation of the movement magnitude component (No Magnitude) did not result in a statistically significant performance change, suggesting that the direction of the suggested movement is more important than its precise scaling in this context. Similarly, removing the basic health reward (No Health) or the repulsion from susceptible individuals (No Susceptible Repulsion) did not significantly impair performance, implying these

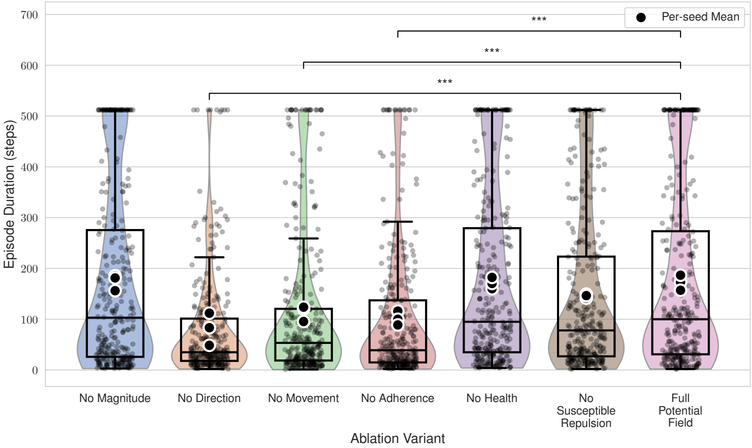

Figure 4: Ablation study of the *Potential Field* reward function. Each variant was evaluated over 100 episodes across 3 training seeds (300 episodes total). Violin plots show the distribution of episode durations, overlaid with boxplots and individual episode results (small black dots). Large black dots with white outlines represent per-seed means. One-sided Mann–Whitney U tests (Bonferroni-corrected) compare each ablation to the full model (*Full Potential Field*), with significance annotations (* $p < 0.05$, ** $p < 0.01$, *** $p < 0.001$) shown for statistically significant differences. See Figure 11 for aggregated means with confidence intervals, and Table 9 for full statistical test results.

components are either less influential or their effects are implicitly captured by other elements of the FPF reward.

Upon removing the adherence reward component (No Adherence), we observed a significant degradation in agent performance. While we might expect agents to implicitly learn the importance of high NPI adherence due to its direct impact on infection risk (especially under simpler reward schemes), this was not what we observed with the complex FPF reward. It is evident from our findings that when a diverse set of reward signals is provided, explicitly rewarding critical behaviors like NPI adherence is crucial for effective learning, as opposed to depending on the policy to deduce their significance. This highlights the importance of careful component weighting and inclusion when engineering sophisticated reward functions for complex tasks.

Comparison of Partial Observability (POMDP) and Full Observability. To understand the learned behavior under limited visibility, we formulate the epidemic control problem as a partially observable Markov decision process (POMDP). In real epidemics, actors have incomplete information about the environment state and infection status of individuals (Gersovitz & Hammer, 2004; Geoffard & Philipson, 1996; Farboodi et al., 2021). We implement this POMDP formulation using a visibility radius constraint, where individuals within radius r of RL agent's position are passed as observations and individuals beyond this radius are unobservable. This natural information asymmetry captures a realistic scenario where agents have limited sensing or information networks that decay with distance. Figure 5 demonstrates trained partial visibility models (r=10, r=15, r=20) paradoxically outperform the baselines and the full visibility trained model, Trained Full, in average reward, episode length and infections per timestep. This counter-intuitive result suggests that complete information can be detrimental to learning, potentially due to observation noise and the increased dimensionality in high-dimensional observation spaces. Limited observability forces the agent to develop more robust strategies and reduces the complexity of the decision space. The trained (Full) model's performance is on par with the greedy heuristic. Notably, a performance differences between r=10, r=15 and r=20 conditions are not statistically significant according to Table 10, indicating a performance plateau beyond a certain visibility threshold.

The POMDP perspective reveals that effective epidemic control strategies can come from local information processing. Agents are able to infer general patterns from partial observations. The improved performance occurring under constrained visibility shows that an information bottleneck can enhance robustness.

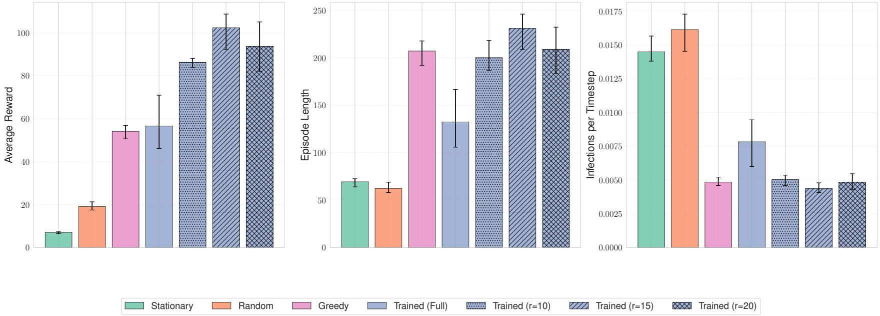

Figure 5: Impact of visibility radius constraints on RL agent performance in epidemic control. The figure compares four agent types across different observation capabilities: Full Visibility (agent observes all infected individuals), and Limited Visibility with radius constraints r=10, r=15, and r=20 (agent only observes infected individuals within the specified radius). Agent types include: Stationary (no movement), Random (random actions), Greedy (heuristic policy avoiding nearest infected), and Trained (PPO-trained RL agents with respective visibility constraints). Results averaged across 3 random seeds with 100 evaluation episodes per seed (N=300 per condition). Error bars show 95% bootstrap confidence intervals from per-seed means. Left: Average cumulative reward per episode. Center: Episode length (survival time in timesteps). Right: Infections per timestep calculated from total infections divided by episode length. Hatching patterns distinguish trained variants: dots (r=10), diagonal lines (r=15), and crosses (r=20). Limited visibility agents (r=15, r=20) achieve higher performance than full visibility, suggesting that observation constraints can improve learning by reducing observation noise and focusing attention on nearby threats.

Social and Economic Constraint in Human Movement. Mobility is a key consideration in epidemiological models (Fakir & Bharati, 2021) and literature review shows that mobility patterns remain unchanged in a pandemic for essential or low wage workers (Gallagher et al., 2021). Inspired by this, we conducted an experiment to evaluate the performance of the agent under these socioeconomic constraints in mobility. Figure 6 shows that the trained PPO agent outperforms stationary, random and greedy baselines when trained on a workplace/home movement cycle. We notice that the stationary and random baselines declined in this cyclic movement, but the trained and greedy baseline improve considerably. Furthermore, the trained RL agent has a higher average reward and higher mean episode length, with an extremely low rate of infections per timestep (Table 2). In the random environment, the agent struggles with long predictions and has a short horizon on its reward, as it performs worse than the greedy baseline. We attribute its inability to beat the local optimization of the greedy algorithm to the noisy observations and movements of the random environment. By incorporating the spatio-temporal regularities of a workplace/home mobility cycle, a trained agent can formulate more effective long-term strategies. The resulting expansion of its planning horizon is empirically validated by a substantial improvement in cumulative average reward over an agent exposed to a random mobility pattern. We anticipated that trained agents operating under cyclic movement patterns would exhibit lower standard deviation across performance metrics compared to those under random movement. However, our results contradicted this expectation. Furthermore, while infections per timestep increased for all agent types, the trained agent demonstrated no such increase, maintaining stable infection rates throughout the evaluation period.

6 Conclusion

We introduced ContagionRL, a novel reinforcement learning platform that enables systematic evaluation of reward function design and for analysis of learned behavior in a spatial epidemics model. Through comprehensive experiments across multiple RL algorithms (PPO, SAC, A2C) and diverse environmental conditions, we show that reward engineering dramatically influences the learned survival strategies. Systematic reward ablations reveal that directional guidance and adherence incentives are essential components for robust policy learning while agents consistently learn adherence to non-pharmaceutical interventions regardless of the reward formulation used for spatial navigation.

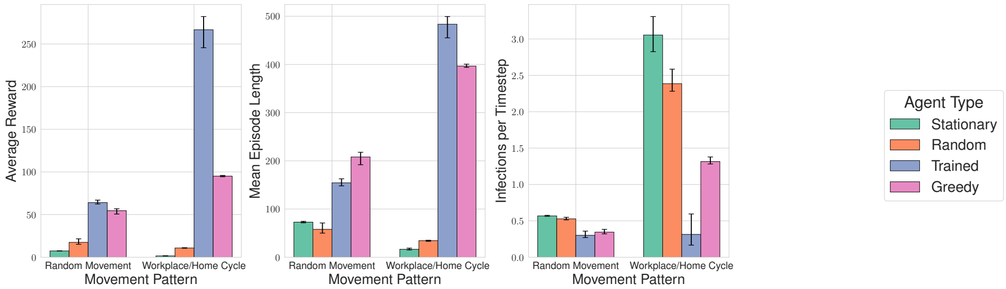

Figure 6: Performance comparison of RL agents across different human movement patterns in epidemic control. The figure shows three metrics across two movement patterns: Random Movement (continuous random walk) and Workplace/Home Cycle (structured movement between workplace and home locations). Four agent types are compared: Stationary, Random, Greedy, and Trained (PPO agent). Results are averaged across 3 random seeds with 100 evaluat ion episodes per seed. Error bars show 95% bootstrap confidence intervals from per-seed means. Left: Average cumulative reward per episode. Center: Mean episode length (survival time). Right: Infection rate. Trained agent significantly outperform all baselines in the Workplace/Home Cycle environment but show mixed results in Random Movement. Statistical results can be found in Table 2

Table 2: Statistical significance tests comparing RL agent performance across movement patterns shown in Figure 6. Trained agents were evaluated using Mann-Whitney U tests with Bonferroni correction for multiple comparisons ($\alpha = 0.05$). Each condition used 300 episodes (3 seeds × 100 episodes per seed). Cross-condition compares trained agents between movement patterns.

Movement Pattern	**Comparison**	**Winner**	**U-stat.**	**p-value**	**Sig.**
Random Movement	Trained vs Stationary	Trained	80,724.0	$p < 0.001$	***
	Trained vs Random	Trained	69,720.0	$p < 0.001$	***
	Trained vs Greedy	Trained	49,117.0	$p = 0.420$	n.s.
Workplace/Home Cycle	Trained vs Stationary	Trained	89,067.0	$p < 0.001$	***
	Trained vs Random	Trained	87,819.0	$p < 0.001$	***
	Trained vs Greedy	Trained	85,853.0	$p < 0.001$	***
Cross-Condition	Trained Random vs Trained Workplace	Workplace	4,100.0	$p < 0.001$	***

We show that different RL algorithms can successfully learn mitigation strategies in the environment. We compare different reward function formulations on performance and structural ablation of reward function design. Also, we find that constraining agent visibility yields superior performance relative to full observability, attributable to reduced dimensional complexity. Furthermore, we reveal structured movement compared to random movement leads to increased longevity of the trained agent. The ContagionRL environment offers insights for developing behaviorally informed epidemic intervention protocols while enabling systematic evaluation of reward function design. It also provides a form of advancing our understanding of how reward structure shapes emergent behaviors in complex spatial and temporal systems such as spatial epidemic models.

References

Michael P. Allen, Dominic J. Tildesley, and Dominic J. Tildesley. *Computer simulation of liquids*. Oxford science publications. Clarendon Pr, Oxford, reprinted edition, 2009. ISBN 9780198556459.

Dario Amodei, Chris Olah, Jacob Steinhardt, Paul Christiano, John Schulman, and Dan Mané. Concrete problems in ai safety. *arXiv preprint arXiv:1606.06565*, 2016.

Mauricio Arango and Lyudmil Pelov. Covid-19 pandemic cyclic lockdown optimization using reinforcement learning. *arXiv preprint arXiv:2009.04647*, 2020.

Kai Arulkumaran, Marc Peter Deisenroth, Miles Brundage, and Anil Anthony Bharath. A brief survey of deep reinforcement learning. *arXiv preprint arXiv:1708.05866*, 2017.

Jonas Balisacan, Monique Chyba, and Corey Shanbrom. Two new compartmental epidemiological models and their equilibria. *medRxiv*, 2021. doi: 10.1101/2021.09.03.21263050. URL https://www.medrxiv.org/content/early/2021/09/07/2021.09.03.21263050.

Shweta Bansal, Bryan T Grenfell, and Lauren Ancel Meyers. When individual behaviour matters: homogeneous and network models in epidemiology. *Journal of the Royal Society Interface*, 4(16):879–891, 2007.

Inan Bostanci and Tim Conrad. Integrating agent-based and compartmental models for infectious disease modeling: A novel hybrid approach. *Journal of Artificial Societies and Social Simulation*, 28(1):5, 2025. ISSN 1460-7425. doi: 10.18564/jasss.5567. URL https://www.jasss.org/28/1/5.html.

Fred Brauer, Carlos Castillo-Chavez, Zhilan Feng, et al. *Mathematical models in epidemiology*, volume 32. Springer, 2019.

Sabah Bushaj, Xuecheng Yin, Arjeta Beqiri, Donald Andrews, and İ. Esra Büyüktahtakın. A simulation-deep reinforcement learning (sirl) approach for epidemic control optimization. *Annals of Operations Research*, 328(1):245–277, September 2023. ISSN 0254-5330, 1572-9338. doi: 10.1007/s10479-022-04926-7. URL https://link.springer.com/10.1007/s10479-022-04926-7.

Nicolò Cangiotti, Marco Capolli, Mattia Sensi, and Sara Sottile. A survey on lyapunov functions for epidemic compartmental models. *Bollettino dell'Unione Matematica Italiana*, 17(2):241–257, June 2024. ISSN 1972-6724, 2198-2759. doi: 10.1007/s40574-023-00368-6. URL https://link.springer.com/10.1007/s40574-023-00368-6.

Ayush Chopra, Esma Gel, Jayakumar Subramanian, Balaji Krishnamurthy, Santiago Romero-Brufau, Kalyan S Pasupathy, Thomas C Kingsley, and Ramesh Raskar. Deepabm: scalable, efficient and differentiable agent-based simulations via graph neural networks. *arXiv preprint arXiv:2110.04421*, 2021.

Monique Chyba, Taylor Klotz, Yuriy Mileyko, and Corey Shanbrom. A look at endemic equilibria of compartmental epidemiological models and model control via vaccination and mitigation. *Mathematics of Control, Signals, and Systems*, 36(2):297–327, June 2024. ISSN 0932-4194, 1435-568X. doi: 10.1007/s00498-023-00365-2. URL https://link.springer.com/10.1007/s00498-023-00365-2.

G. Dimarco, B. Perthame, G. Toscani, and M. Zanella. Kinetic models for epidemic dynamics with social heterogeneity. *Journal of Mathematical Biology*, 83(1):4, July 2021. ISSN 0303-6812, 1432-1416. doi: 10.1007/s00285-021-01630-1. URL https://link.springer.com/10.1007/s00285-021-01630-1.

Xinqi Du, Hechang Chen, Bo Yang, Cheng Long, and Songwei Zhao. Hrl4ec: Hierarchical reinforcement learning for multi-mode epidemic control. *Information Sciences*, 640:119065, 2023.

Adnan M. S. Fakir and Tushar Bharati. Pandemic catch-22: The role of mobility restrictions and institutional inequalities in halting the spread of covid-19. *PLOS ONE*, 16(6):e0253348, June 2021. ISSN 1932-6203. doi: 10.1371/journal.pone.0253348. URL http://dx.doi.org/10.1371/journal.pone.0253348.

Maryam Farboodi, Gregor Jarosch, and Robert Shimer. Internal and external effects of social distancing in a pandemic. *Journal of Economic Theory*, 196:105293, 2021.

Tao Feng, Tong Xia, Xiaochen Fan, Huandong Wang, Zefang Zong, and Yong Li. Precise mobility intervention for epidemic control using unobservable information via deep reinforcement learning. In *Proceedings of the 28th ACM SIGKDD Conference on Knowledge Discovery and Data Mining*, pp. 2882–2892, 2022.

Tao Feng, Sirui Song, Tong Xia, and Yong Li. Contact tracing and epidemic intervention via deep reinforcement learning. *ACM Transactions on Knowledge Discovery from Data*, 17(3):1–24, 2023.

Neil M Ferguson, Daniel Laydon, Gemma Nedjati-Gilani, Natsuko Imai, Kylie Ainslie, Marc Baguelin, Sangeeta Bhatia, Adhiratha Boonyasiri, Zulma Cucunubá, Gina Cuomo-Dannenburg, et al. *Report 9: Impact of non-pharmaceutical interventions (NPIs) to reduce COVID19 mortality and healthcare demand*, volume 16. Imperial College London London, 2020.

Jakob Foerster, Nantas Nardelli, Gregory Farquhar, Triantafyllos Afouras, Philip HS Torr, Pushmeet Kohli, and Shimon Whiteson. Stabilising experience replay for deep multi-agent reinforcement learning. In *International conference on machine learning*, pp. 1146–1155. PMLR, 2017.

Vincent François-Lavet, Peter Henderson, Riashat Islam, Marc G Bellemare, Joelle Pineau, et al. An introduction to deep reinforcement learning. *Foundations and Trends® in Machine Learning*, 11(3-4): 219–354, 2018.

Daan Frenkel and Berend Smit. *Understanding molecular simulation: from algorithms to applications*. Computational science series. Academic press, San Diego, 2nd ed edition, 2002. ISBN 9780122673511.

Avner Friedman and Chiu-Yen Kao. *Mathematical modeling of biological processes*, volume 1. Springer, 2014.

Sebastian Funk, Marcel Salathé, and Vincent AA Jansen. Modelling the influence of human behaviour on the spread of infectious diseases: a review. *Journal of the Royal Society Interface*, 7(50):1247–1256, 2010.

Susan Gallagher, Asha Roy, Sandra J. Domeracki, Todd Mohrmann, Vicki Missar, Janet Jule, Shreela Sharma, and Ryan DeWitt. The low-wage essential worker: Occupational concerns and needs in the covid-19 pandemic—a round table. *Workplace Health & Safety*, 69(4):154–160, March 2021. ISSN 2165-0969. doi: 10.1177/2165079920988682. URL http://dx.doi.org/10.1177/2165079920988682.

Pierre-Yves Geoffard and Tomas Philipson. Rational epidemics and their public control. *International economic review*, pp. 603–624, 1996.

Mark Gersovitz and Jeffrey S Hammer. The economical control of infectious diseases. *The Economic Journal*, 114(492):1–27, 2004.

Volker Grimm and Steven F Railsback. Individual-based modeling and ecology. In *Individual-based modeling and ecology*. Princeton university press, 2013.

Tuomas Haarnoja, Aurick Zhou, Pieter Abbeel, and Sergey Levine. Soft actor-critic: Off-policy maximum entropy deep reinforcement learning with a stochastic actor. In *International conference on machine learning*, pp. 1861–1870. Pmlr, 2018.

Herbert W Hethcote. The mathematics of infectious diseases. *SIAM review*, 42(4):599–653, 2000.

Elizabeth Hunter, Brian Mac Namee, and John D. Kelleher. A taxonomy for agent-based models in human infectious disease epidemiology. *Journal of Artificial Societies and Social Simulation*, 20(3):2, 2017. ISSN 1460-7425. doi: 10.18564/jasss.3414. URL http://jasss.soc.surrey.ac.uk/20/3/2.html.

Elizabeth Hunter, Brian Mac Namee, and John Kelleher. An open-data-driven agent-based model to simulate infectious disease outbreaks. *PLOS ONE*, 13(12):e0208775, December 2018. ISSN 1932-6203. doi: 10.1371/journal.pone.0208775. URL https://dx.plos.org/10.1371/journal.pone.0208775.

Sinan Ibrahim, Mostafa Mostafa, Ali Jnadi, Hadi Salloum, and Pavel Osinenko. Comprehensive overview of reward engineering and shaping in advancing reinforcement learning applications. *IEEE Access*, 12: 175473–175500, 2024. doi: 10.1109/ACCESS.2024.3504735.

Ning Jiang, Weiqi Chu, and Yao Li. Modeling, inference, and prediction in mobility-based compartmental models for epidemiology. *ArXiv*, abs/2406.12002, 2024. URL `https://api.semanticscholar.org/CorpusID:270562555`.

Matt J. Keeling and Pejman Rohani. *Modeling Infectious Diseases in Humans and Animals.* Princeton University Press, 2008. ISBN 9780691116174. URL `http://www.jstor.org/stable/j.ctvcm4gk0`.

William Ogilvy Kermack and Anderson G McKendrick. A contribution to the mathematical theory of epidemics. *Proceedings of the royal society of london. Series A, Containing papers of a mathematical and physical character*, 115(772):700–721, 1927.

Harshad Khadilkar, Tanuja Ganu, and Deva P Seetharam. Optimising lockdown policies for epidemic control using reinforcement learning: An ai-driven control approach compatible with existing disease and network models. *Transactions of the Indian National Academy of Engineering*, 5(2):129–132, 2020.

Lingcai Kong, Jinfeng Wang, Weiguo Han, and Zhidong Cao. Modeling heterogeneity in direct infectious disease transmission in a compartmental model. *International Journal of Environmental Research and Public Health*, 13(3):253, February 2016. ISSN 1660-4601. doi: 10.3390/ijerph13030253. URL `https://www.mdpi.com/1660-4601/13/3/253`.

Gloria Hyunjung Kwak, Lowell Ling, and Pan Hui. Deep reinforcement learning approaches for global public health strategies for covid-19 pandemic. *PloS one*, 16(5):e0251550, 2021.

Joel Z Leibo, Vinicius Zambaldi, Marc Lanctot, Janusz Marecki, and Thore Graepel. Multi-agent reinforcement learning in sequential social dilemmas. *arXiv preprint arXiv:1702.03037*, 2017.

Yuxi Li. Deep reinforcement learning: An overview. *arXiv preprint arXiv:1701.07274*, 2017.

Pieter JK Libin, Arno Moonens, Timothy Verstraeten, Fabian Perez-Sanjines, Niel Hens, Philippe Lemey, and Ann Nowé. Deep reinforcement learning for large-scale epidemic control. In *Machine Learning and Knowledge Discovery in Databases. Applied Data Science and Demo Track: European Conference, ECML PKDD 2020, Ghent, Belgium, September 14–18, 2020, Proceedings, Part V*, pp. 155–170. Springer, 2021.

Anh Mai, Nikunj Gupta, Azza Abouzied, and Dennis Shasha. Planning multiple epidemic interventions with reinforcement learning. In *Proceedings of the Thirty-Second International Joint Conference on Artificial Intelligence*, pp. 6147–6155, Macau, SAR China, August 2023. International Joint Conferences on Artificial Intelligence Organization. ISBN 9781956792034. doi: 10.24963/ijcai.2023/682. URL `https://www.ijcai.org/proceedings/2023/682`.

Piero Manfredi and Alberto D'Onofrio. *Modeling the interplay between human behavior and the spread of infectious diseases.* Springer Science & Business Media, 2013.

Susanna Manrubia and Damián H Zanette. Individual risk-aversion responses tune epidemics to critical transmissibility (r= 1). *Royal Society Open Science*, 9(4):211667, 2022.

Volodymyr Mnih, Koray Kavukcuoglu, David Silver, Andrei A Rusu, Joel Veness, Marc G Bellemare, Alex Graves, Martin Riedmiller, Andreas K Fidjeland, Georg Ostrovski, et al. Human-level control through deep reinforcement learning. *nature*, 518(7540):529–533, 2015.

Volodymyr Mnih, Adria Puigdomenech Badia, Mehdi Mirza, Alex Graves, Timothy Lillicrap, Tim Harley, David Silver, and Koray Kavukcuoglu. Asynchronous methods for deep reinforcement learning. In Maria Florina Balcan and Kilian Q. Weinberger (eds.), *Proceedings of The 33rd International Conference on Machine Learning*, volume 48 of *Proceedings of Machine Learning Research*, pp. 1928–1937, New York, New York, USA, 20–22 Jun 2016. PMLR. URL `https://proceedings.mlr.press/v48/mniha16.html`.

Seyed Sajad Mousavi, Michael Schukat, and Enda Howley. Deep reinforcement learning: an overview. In *Proceedings of SAI intelligent systems conference*, pp. 426–440. Springer, 2016.

Andrew Y Ng, Daishi Harada, and Stuart Russell. Policy invariance under reward transformations: Theory and application to reward shaping. In *Icml*, volume 99, pp. 278–287. Citeseer, 1999.

Tai Nguyen, Phong Le, André Biedenkapp, Carola Doerr, and Nguyen Dang. *On the Importance of Reward Design in Reinforcement Learning-based Dynamic Algorithm Configuration: A Case Study on OneMax with (1+(λ,λ))-GA*, pp. 1162–1171. Association for Computing Machinery, New York, NY, USA, 2025. ISBN 9798400714658. URL https://doi.org/10.1145/3712256.3726395.

Joon Sung Park, Joseph O'Brien, Carrie Jun Cai, Meredith Ringel Morris, Percy Liang, and Michael S Bernstein. Generative agents: Interactive simulacra of human behavior. In *Proceedings of the 36th annual acm symposium on user interface software and technology*, pp. 1–22, 2023.

Antonin Raffin, Ashley Hill, Adam Gleave, Anssi Kanervisto, Maximilian Ernestus, and Noah Dormann. Stable-baselines3: Reliable reinforcement learning implementations. *Journal of Machine Learning Research*, 22(268):1–8, 2021. URL http://jmlr.org/papers/v22/20-1364.html.

Rubina F Rizvi, Kelly J Thomas Craig, Rezzan Hekmat, Fredy Reyes, Brett South, Bedda Rosario, William J Kassler, and Gretchen P Jackson. Effectiveness of non-pharmaceutical interventions related to social distancing on respiratory viral infectious disease outcomes: A rapid evidence-based review and meta-analysis. *SAGE Open Med.*, 9:20503121211022973, June 2021.

Christopher Rose, Andrew J. Medford, C. Franklin Goldsmith, Tejs Vegge, Joshua S. Weitz, and Andrew A. Peterson. Heterogeneity in susceptibility dictates the order of epidemic models. *Journal of Theoretical Biology*, 528:110839, November 2021. ISSN 00225193. doi: 10.1016/j.jtbi.2021.110839. URL https://linkinghub.elsevier.com/retrieve/pii/S0022519321002587.

Chadi M Saad-Roy and Arne Traulsen. Dynamics in a behavioral–epidemiological model for individual adherence to a nonpharmaceutical intervention. *Proceedings of the National Academy of Sciences*, 120(44): e2311584120, 2023.

John Schulman, Filip Wolski, Prafulla Dhariwal, Alec Radford, and Oleg Klimov. Proximal policy optimization algorithms. *arXiv preprint arXiv:1707.06347*, 2017.

Ibne Farabi Shihab, Sanjeda Akter, and Anuj Sharma. Detecting and mitigating reward hacking in reinforcement learning systems: A comprehensive empirical study, 2025. URL https://arxiv.org/abs/2507.05619.

Alexander F. Siegenfeld, Pratyush K. Kollepara, and Yaneer Bar-Yam. Modeling complex systems: A case study of compartmental models in epidemiology. *Complexity*, 2022(1):3007864, January 2022. ISSN 1076-2787, 1099-0526. doi: 10.1155/2022/3007864. URL https://onlinelibrary.wiley.com/doi/10.1155/2022/3007864.

David Silver, Aja Huang, Chris J Maddison, Arthur Guez, Laurent Sifre, George Van Den Driessche, Julian Schrittwieser, Ioannis Antonoglou, Veda Panneershelvam, Marc Lanctot, et al. Mastering the game of go with deep neural networks and tree search. *nature*, 529(7587):484–489, 2016.

Tarini Sudhakar, Ashna Bhansali, John Walkington, and David Puelz. The disutility of compartmental model forecasts during the covid-19 pandemic. *Frontiers in Epidemiology*, 4:1389617, June 2024. ISSN 2674-1199. doi: 10.3389/fepid.2024.1389617. URL https://www.frontiersin.org/articles/10.3389/fepid.2024.1389617/full.

Richard S. Sutton and Andrew G. Barto. *Reinforcement learning: an introduction.* Adaptive computation and machine learning series. The MIT Press, Cambridge, Massachusetts, second edition edition, 2018. ISBN 9780262039246.

Ardi Tampuu, Tambet Matiisen, Dorian Kodelja, Ilya Kuzovkin, Kristjan Korjus, Juhan Aru, Jaan Aru, and Raul Vicente. Multiagent cooperation and competition with deep reinforcement learning. *PloS one*, 12(4): e0172395, 2017.

Mark Towers, Ariel Kwiatkowski, Jordan Terry, John U Balis, Gianluca De Cola, Tristan Deleu, Manuel Goulao, Andreas Kallinteris, Markus Krimmel, Arjun KG, et al. Gymnasium: A standard interface for reinforcement learning environments. *arXiv preprint arXiv:2407.17032*, 2024.

Melissa Tracy, Magdalena Cerdá, and Katherine M. Keyes. Agent-based modeling in public health: Current applications and future directions. *Annual Review of Public Health*, 39(1):77–94, April 2018. ISSN 0163-7525, 1545-2093. doi: 10.1146/annurev-publhealth-040617-014317. URL `https://www.annualreviews.org/content/journals/10.1146/annurev-publhealth-040617-014317`.

Runzhe Wan, Xinyu Zhang, and Rui Song. Multi-objective model-based reinforcement learning for infectious disease control. In *Proceedings of the 27th ACM SIGKDD Conference on Knowledge Discovery and Data Mining*, pp. 1634–1644, Virtual Event Singapore, August 2021. ACM. ISBN 9781450383325. doi: 10.1145/3447548.3467303. URL `https://dl.acm.org/doi/10.1145/3447548.3467303`.

Bing Wang, Zeyang Xie, and Yuexing Han. Impact of individual behavioral changes on epidemic spreading in time-varying networks. *Physical Review E*, 104(4):044307, 2021.

Zhen Wang, Chris T Bauch, Samit Bhattacharyya, Alberto d'Onofrio, Piero Manfredi, Matjaž Perc, Nicola Perra, Marcel Salathé, and Dawei Zhao. Statistical physics of vaccination. *Physics Reports*, 664:1–113, 2016.

Edwin B Wilson and Jane Worcester. The law of mass action in epidemiology. *Proceedings of the National Academy of Sciences*, 31(1):24–34, 1945.

Yang Ye, Qingpeng Zhang, Zhongyuan Ruan, Zhidong Cao, Qi Xuan, and Daniel Dajun Zeng. Effect of heterogeneous risk perception on information diffusion, behavior change, and disease transmission. *Physical review E*, 102(4):042314, 2020.

Cameron Zachreson, Sheryl Chang, Nathan Harding, and Mikhail Prokopenko. The effects of local homogeneity assumptions in metapopulation models of infectious disease. *Royal Society Open Science*, 9(7):211919, 2022.

Appendix

A Compartmental Epidemiology Models Continued

A.1 Notation and parameter definitions

We denote by the numbers of susceptible, infected, recovered, exposed and deceased individuals at time t using $S(t)$, $I(t)$, $R(t)$, $E(t)$, $D(t)$, respectively. In the SIR, SIRS and SIRS+D models the total living population is

$$N(t) = S(t) + I(t) + R(t), \tag{3}$$

whereas in the SEIR model

$$N(t) = S(t) + E(t) + I(t) + R(t), \tag{4}$$

The model parameters are:

β transmission rate (per-contact rate at which susceptibles become infected);

γ recovery rate (rate at which infected individuals recover);

σ progression rate (rate at which exposed become infectious, SEIR only);

ξ immunity-waning rate (rate at which recovered lose immunity, SIRS and SIRS+D);

μ disease-induced mortality rate (rate at which infected die, SIRS+D only).

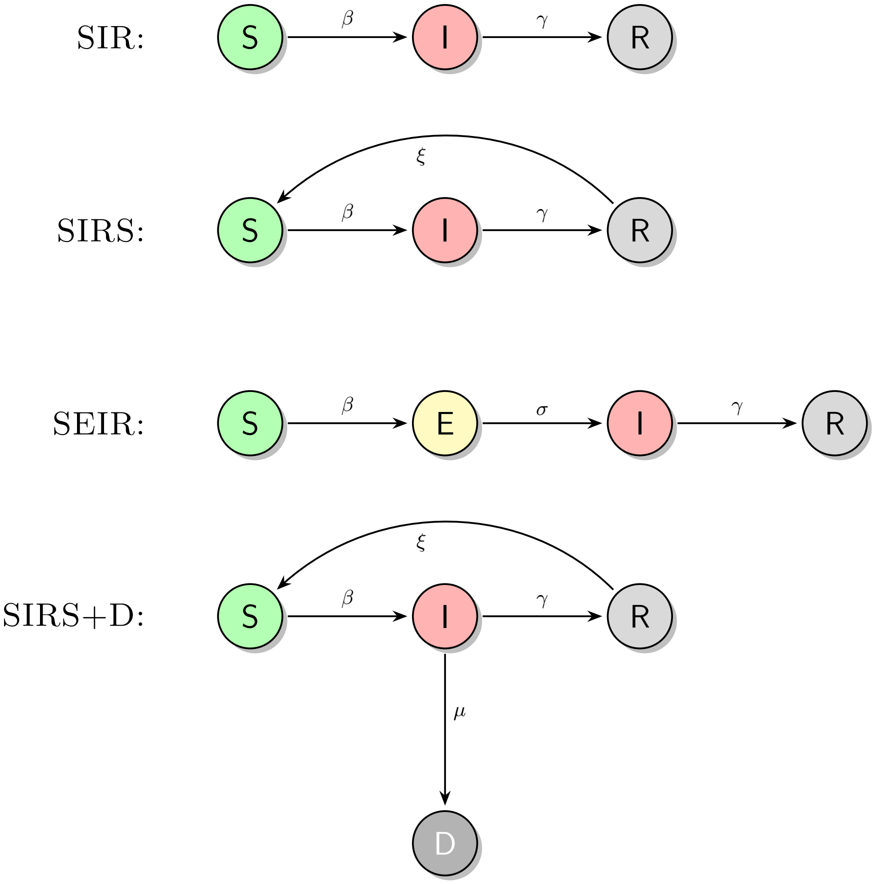

Figure 7: Compartmental epidemic models visualized: SIR, SIRS, SEIR, and SIRS+D.

A.2 Model equations

The differential equations below provide an overview of how compartments are tracked and changed population-wide based on the defined respective parameters in Appendix A.1.

SIR model.

$$\frac{dS}{dt} = -\beta\,\frac{SI}{N}, \tag{5}$$
$$\frac{dI}{dt} = \beta\,\frac{SI}{N} - \gamma\,I, \tag{6}$$
$$\frac{dR}{dt} = \gamma\,I. \tag{7}$$

SIRS model.

$$\frac{dS}{dt} = -\beta\,\frac{SI}{N} + \xi\,R, \tag{8}$$
$$\frac{dI}{dt} = \beta\,\frac{SI}{N} - \gamma\,I, \tag{9}$$
$$\frac{dR}{dt} = \gamma\,I - \xi\,R. \tag{10}$$

SEIR model.

$$\frac{dS}{dt} = -\beta\,\frac{SI}{N}, \tag{11}$$
$$\frac{dE}{dt} = \beta\,\frac{SI}{N} - \sigma\,E, \tag{12}$$
$$\frac{dI}{dt} = \sigma\,E - \gamma\,I, \tag{13}$$
$$\frac{dR}{dt} = \gamma\,I. \tag{14}$$

SIRS+D model.

$$\frac{dS}{dt} = -\beta\,\frac{SI}{N} + \xi\,R, \tag{15}$$
$$\frac{dI}{dt} = \beta\,\frac{SI}{N} - (\gamma + \mu)\,I, \tag{16}$$
$$\frac{dR}{dt} = \gamma\,I - \xi\,R, \tag{17}$$
$$\frac{dD}{dt} = \mu\,I. \tag{18}$$

A.3 Comparison of the epidemiological models

Table 3: Comparison of epidemic models and their capacity for individual-level and adaptive behavior modeling

Model	Compartments	Reinfection	Incubation	Death	Behavioral Modeling	Adaptive Behavior Modeling
SIR (Kermack & McKendrick, 1927)	S, I, R	No	No	No	None	No
SIRS (Kermack & McKendrick, 1927)	S, I, R	Yes	No	No	None	No
SEIR (Kermack & McKendrick, 1927; Wilson & Worcester, 1945)	S, E, I, R	No	Yes	No	None	No
SIRS+D (Wilson & Worcester, 1945)	S, I, R, D	Yes	No	Yes	None	No
ABM (Grimm & Railsback, 2013)	Custom per agent	Yes	Optional	Yes	**Prescribed rules**	Partial
ContagionRL	**Modified SIRS+D**	**Yes**	**No**	**Yes**	**Learned policies (RL)**	**Yes**

B Environment Visualization

Figure 8 shows a single frame of the environment's rendered video. The visualization provides a comprehensive and intuitive overview of the simulation state and the environment at each timestep. The panel at the center shows the environment's grid, in which each human is represented as a colored circle depending on its epidemiological state. The legend is shown on the left of the grid (blue for susceptible, red for infectious, green for recovered, and gray for dead). The focal agent, whose actions are being learned by RL, is shown as a orange dot with dark border. The small arrow, originating from the agent, shows its most recent movement direction and magnitude.

The upper panel on the right of the grid, shows the details related to the agent such as current state, position, adherence level, and cumulative reward. While the panel below it shows the population distribution across all epidemiological states in numbers and absolute percentages (due to increased need of processing power for rendering this function is turned off by default).

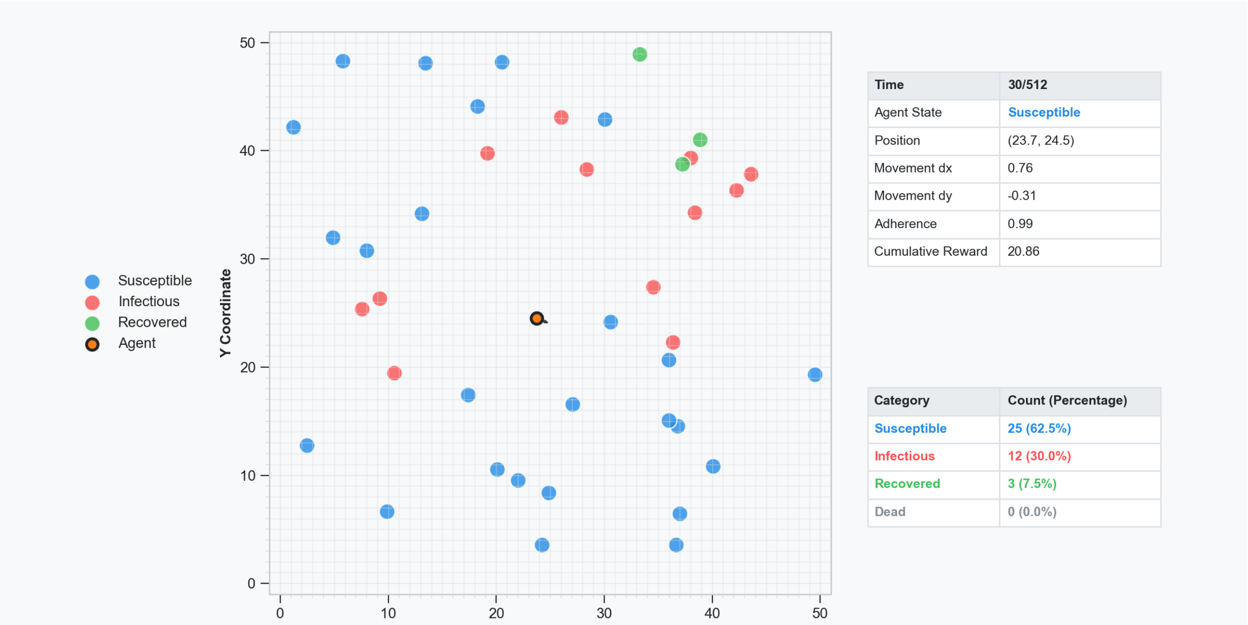

Time	30/512
Agent State	Susceptible
Position	(23.7, 24.5)
Movement dx	0.76
Movement dy	-0.31
Adherence	0.99
Cumulative Reward	20.86

Category	Count (Percentage)
Susceptible	25 (62.5%)
Infectious	12 (30.0%)
Recovered	3 (7.5%)
Dead	0 (0.0%)

Figure 8: Sample render of the SIRS+D environment at step 30 of an episode

C Methodology Continued

C.1 Toroidal Distance Calculation

Throughout the simulation, distances between individuals are calculated using the standard Euclidean distance metric, modified to account for the periodic boundary conditions of the toroidal grid. This ensures that the distance represents the shortest path, considering potential "wrap-around" across grid edges.

The distance $d(i, j)$ between two individuals i and j at positions (x_i, y_i) and (x_j, y_j) respectively, within a grid of side length G, is calculated as:

$$d(i, j) = \sqrt{\Delta x_{\text{wrap}}^2 + \Delta y_{\text{wrap}}^2} \tag{19}$$

where the wrapped differences along each axis are determined by:

$$\Delta x_{\text{wrap}} = \min(|x_i - x_j|, G - |x_i - x_j|), \Delta y_{\text{wrap}} = \min(|y_i - y_j|, G - |y_i - y_j|) \tag{20}$$

This formulation ensures that the distance along each dimension corresponds to the shorter of the two possible paths (direct or wrapped around the grid). This distance metric is fundamental to calculating infection exposure, determining the nearest threat for the Greedy policy, and computing forces in the potential field reward function.

C.2 Environment Configuration Details

For completeness and to ensure the reproducibility of our experiments, this section provides a detailed breakdown of the specific parameter values used to configure the SIRS+D simulation environment described in section 3. Table 4 lists each parameter, its corresponding symbol used within the text (where applicable), its configured value, and a brief description of its role within the simulation dynamics. These parameters define the epidemiological characteristics, spatial properties, and agent interaction rules governing the environment used throughout our study.

Table 4: SIRS+D Environment Configuration Parameters

Parameter	Value	Type	Range	Description
Simulation Time	512	integer	$[1, \infty)$	Maximum number of timesteps per episode.
Grid Size	50	integer	$[1, \infty)$	Side length of the square, toroidal grid (Value x Value).
Number of Humans	40	integer	$[0, \infty)$	Number of non-agent individuals in the simulation.
Initial Infected	10	integer	$[0, 40]$	Number of initially infected individuals (up to Number of Humans).
Infection Rate	0.5	float	$[0, 1]$	Base infection transmission rate per exposure unit.
Initial Agent Adherence	0	float	$[0, 1]$	Agent's NPI adherence level at the start of an episode.
Distance Decay	0.3	float	$[0, \infty)$	Exponential decay factor for infection exposure based on distance.
Lethality Rate	0	float	$[0, 1]$	Per-step probability of death for infected individuals.
Immunity Loss Probability	0.25	float	$[0, 1]$	Per-step probability of transitioning from Recovered (R) to Susceptible (S).
Recovery Rate	0.1	float	$[0, 1]$	Per-step probability of transitioning from Infected (I) to Recovered (R).
Adherence Penalty Factor	1	float	$[1, \infty)$	Multiplicative factor for adherence cost (used by some reward functions).
Adherence Effectiveness	0.2	float	$[0, 1]$	Residual transmission factor when agent adherence is 1.0 (e.g., 0.2 means 20% of beta remains).
Movement Type	`continuous_random`	string	Categorical	Movement model for non-agent individuals (e.g., `continuous_random`).
Movement Scale	1	float	$[0, 1]$	Maximum step size scale for non-agent individuals.
Visibility Radius	-1	float	$\{-1\} \cup [0, \infty)$	Agent's observation radius (-1 indicates full grid visibility).
Reinfection Count	5	integer	$[0, \infty)$	Number of S individuals reinfected if $I_t = 0$.
Safe Distance	10	float	$[0, \infty)$	Min distance for (re)infecting S individuals relative to the agent.
Initial Agent Distance	5	float	$[0, \infty)$	Min distance all individuals are placed from the agent at initialization.
Max Infection Distance	10	float	$\{-1\} \cup (0, \infty)$	Max distance for an infected individual to contribute to exposure (-1 for infinite).
Reward Function Type	`potential_field`	string	Categorical	Identifier for the reward function (e.g., `potential_field`, `sparse`).
Reward Ablation	`full`	string	Categorical	Specifies variant of reward function for ablation studies (e.g., `full`, `no_health`).
Render Mode	`None`	string or NoneType	{`rgb_array`, `None`}	Rendering mode for visualization.

C.3 Reward Function Implementation Details

This appendix provides the detailed mathematical formulations for key reward functions implemented in the ContagionRL environment. The goal of the agent, in the context of these reward functions, is to maximize the cumulative reward, which is designed to correlate with prolonging its susceptible state.

C.3.1 Constant Reward

This is the simplest reward structure, providing a binary signal based on the agent's health state. Let S_a denote the state of the agent. The reward R_{const} at each timestep is defined as:

$$R_{\text{const}} = \begin{cases} 1 & \text{if } S_a = \text{Susceptible} \\ 0 & \text{otherwise} \end{cases} \tag{21}$$

C.3.2 Reduce Infection Probability Reward

This reward function directly incentivizes the agent to minimize its own probability of becoming infected. Let $P_{\text{infect}}(a)$ be the agent's probability of infection at the current timestep, calculated considering its position, adherence, and proximity to infected individuals. The reward $R_{\text{reduce\_inf}}$ is defined as:

$$R_{\text{reduce\_inf}} = \begin{cases} (1 - P_{\text{infect}}(a))^2 & \text{if } S_a = \text{Susceptible} \\ -5 & \text{if } S_a \neq \text{Susceptible} \end{cases} \tag{22}$$

The quadratic term $(1 - P_{\text{infect}}(a))^2$ strongly rewards states with very low infection probability.

C.3.3 Combined Reward

This function combines the incentive to reduce infection probability with a small constant bonus for remaining susceptible. Using $P_{\text{infect}}(a)$ as defined above, and R_{const} (which is 1 if susceptible, 0 otherwise from the agent's perspective in this formulation if it's not infected):

$$R_{\text{combo}} = \begin{cases} 0.8 \cdot (1 - P_{\text{infect}}(a))^2 + 0.1 & \text{if } S_a = \text{Susceptible} \\ 0 & \text{if } S_a \neq \text{Susceptible} \end{cases} \tag{23}$$

The 0.1 term derives from $0.1 \times R_{\text{const}}$ where $R_{\text{const}} = 1$ when the agent is susceptible.

C.3.4 Maximize Nearest Distance Reward

This reward encourages the agent to maintain a certain distance from other individuals, primarily those who are susceptible or infected. Let d_{min} be the Euclidean distance from the agent to the nearest human h whose state $S_h \in \{\text{Susceptible, Infected}\}$. Let D_β be the parameter maximum distance for beta calculation from the environment configuration. The reward $R_{\text{max\_dist}}$ is defined as:

$$R_{\text{max\_dist}} = \begin{cases} 0 & \text{if } S_a = \text{Infected} \\ 1 & \text{if } S_a \neq \text{Infected and no relevant humans (S or I) exist} \\ 1 & \text{if } S_a \neq \text{Infected and } d_{\text{min}} \geq D_\beta \text{ (and } D_\beta > 0) \\ \max(0, d_{\text{min}}/D_\beta) & \text{if } S_a \neq \text{Infected and } d_{\text{min}} < D_\beta \text{ (and } D_\beta > 0) \end{cases} \tag{24}$$

If $D_\beta \leq 0$ (interpreted as infinite or disabled threshold in some contexts, though the code uses it as a divisor if positive), the behavior might implicitly rely on normalization or other logic not explicitly captured by this simplified $D_\beta > 0$ case. The provided code primarily gives reward based on d_{min}/D_β when $d_{\text{min}} < D_\beta$ and $D_\beta > 0$.

C.3.5 Potential Field Reward

The Potential Field reward function conceptualizes agent-human interactions as a system of forces, guiding the agent's movement based on the proximity and state of other individuals. It is a composite reward with several terms:

$$R_{\text{PF}} = w_{\text{health}} r_{\text{health}} + w_{\text{adherence}} r_{\text{adherence}} + w_{\text{movement}} r_{\text{move}} \tag{25}$$

In the implementation, the weights are $w_{\text{health}} = 0.1$, $w_{\text{adherence}} = 0.2$, and $w_{\text{movement}} = 0.7$.

1. Health Reward (r_{health}): This is a binary reward for maintaining a susceptible state.

$$r_{\text{health}} = \begin{cases} 1 & \text{if } S_a = \text{Susceptible} \\ 0 & \text{otherwise} \end{cases} \tag{26}$$

(This component can be ablated to 0 via the no health variant).

2. Adherence Reward ($r_{\text{adherence}}$): This reward is directly proportional to the agent's NPI adherence level. Let α_a be the agent's current adherence (a value in $[0, 1]$).

$$r_{\text{adherence}} = \alpha_a \tag{27}$$

(This component can be ablated to 0 via the no adherence variant).

3. Movement Reward (r_{move}): This component rewards the agent for moving in alignment with a suggested force vector $\mathbf{F}$ and optionally for matching its magnitude. Let the agent's current position be $\mathbf{p}_a = (x_a, y_a)$ and human j's position be $\mathbf{p}_j = (x_j, y_j)$. The shortest displacement vector on the toroidal grid from human j to the agent is $\Delta\mathbf{p}_j = (\Delta x_j, \Delta y_j)$, where:

$$\Delta x_j = (x_a - x_j + G/2) \pmod G - G/2 \tag{28}$$

$$\Delta y_j = (y_a - y_j + G/2) \pmod G - G/2 \tag{29}$$

Here, G is the grid size. The squared distance is $d_j^2 = (\Delta x_j)^2 + (\Delta y_j)^2 + \epsilon_{\text{dist}}$, where ϵ_{dist} is a small constant to prevent division by zero.

The force contribution from each human j depends on its state:

$$\text{weight}_j = \begin{cases} W_I & \text{if human } j \text{ is Infected (I)} \\ W_S & \text{if human } j \text{ is Susceptible (S) (can be 0 in no Susceptible ablation)} \\ 0 & \text{otherwise} \end{cases} \tag{30}$$

The scaling factor for the force from human j is $\text{scale}_j = \text{weight}_j/(d_j^2)^{p/2}$. The implementation uses $p = 1$, $W_I = 1.0$, $W_S = 0.5$. The resultant force vector is $\mathbf{F} = (F_x, F_y) = \sum_j \text{scale}_j \Delta\mathbf{p}_j$. The normalized force direction is $\hat{\mathbf{F}} = \mathbf{F}/(\|\mathbf{F}\| + \epsilon_{\text{norm}})$.

Let the agent's chosen movement vector from the last action be $\mathbf{a} = (a_x, a_y)$. The directional alignment reward is:

$$r_{\text{dir}} = \text{clip}\left(\frac{\mathbf{a} \cdot \hat{\mathbf{F}}}{\|\mathbf{a}\| + \epsilon_{\text{norm}}}, -1, 1\right) \tag{31}$$

The magnitude matching reward is:

$$r_{\text{mag}} = \text{clip}(1 - |\|\mathbf{a}\| - \min(\|\mathbf{F}\|, 1.0)|, -1, 1) \tag{32}$$

The combined movement reward is (by default, with $\beta_m = 0.25$):

$$r_{\text{move}} = (1 - \beta_m)r_{\text{dir}} + \beta_m r_{\text{mag}} \tag{33}$$

This term is subject to ablations:

- *No Magnitude*: $r_{\text{move}} = r_{\text{dir}}$
- *No Direction*: $r_{\text{move}} = r_{\text{mag}}$
- *No Movement*: $r_{\text{move}} = 0$

The small constants ϵ_{dist} and ϵ_{norm} (10^{-8}) are used to ensure numerical stability.

C.4 Algorithmic Comparison Hyperparameters

The following tables summarize the hyperparameters used for the Proximal Policy Optimization (PPO), Soft Actor-Critic (SAC), and Advantage Actor-Critic (A2C) algorithms in our comparative study (Figure 2).

Table 5: PPO Hyperparameters

Hyperparameter	Value
Policy Type	`MultiInputPolicy`
Policy Kwargs:	
Net Arch (pi)	`[256, 256, 256, 256]`
Net Arch (vf)	`[256, 256, 256, 256]`
Activation Fn	`ReLU`
Ortho Init	`True`
Batch Size	2048
N Steps	1024
N Epochs	5
Learning Rate	`3e-4`
Gamma	0.96
GAE Lambda	0.95
Target KL	0.04
Clip Range	0.2
Ent Coef	0.02
Normalize Advantage	`True`
Total Timesteps	8,000,000
N Envs	4

Table 6: SAC Hyperparameters

Hyperparameter	Value
Policy Type	`MlpPolicy`
Policy Kwargs:	
Net Arch (pi)	`[256, 256, 256, 256]`
Net Arch (qf)	`[256, 256, 256, 256]`
Activation Fn	`ReLU`
Learning Rate	`3e-4`
Buffer Size	1,000,000
Batch Size	256
Tau	0.005
Train Freq	1
Gradient Steps	1
Ent Coef	`auto`
Gamma	0.96
Total Timesteps	8,000,000
N Envs	4

Table 7: A2C Hyperparameters

Hyperparameter	Value
Policy Type	`MlpPolicy`
Policy Kwargs:	
Net Arch (pi)	`[256, 256, 256, 256]`
Net Arch (vf)	`[256, 256, 256, 256]`
Activation Fn	`ReLU`
Ortho Init	`True`
N Steps	640
Gamma	0.96
GAE Lambda	0.95
Ent Coef	0.01
VF Coef	0.5
Max Grad Norm	0.5
Learning Rate	`3e-4`
Use RMS Prop	`True`
Normalize Advantage	`True`
Total Timesteps	8,000,000
N Envs	4

C.5 Baseline Implementation Details

This section provides further detail on the implementation of the non-learning baseline policies used for comparative analysis, as described in Section 4.

C.5.1 Stationary Policy Implementation

The Stationary policy represents a minimal activity baseline. Its implementation is deterministic: at every timestep t within an episode, the agent selects a constant action vector $a(t) = [0.0, 0.0, 0.0]$. This corresponds to zero intended movement ($\Delta x = 0, \Delta y = 0$) and zero NPI adherence ($\alpha = 0$). The agent's position remains fixed, and its susceptibility is solely determined by the base infection rate β and its exposure to infected individuals based on the environment dynamics.

C.5.2 Random Policy Implementation

The Random policy simulates behavior devoid of environmental feedback or strategy. At each timestep t, the action $a(t) = (\Delta x, \Delta y, \alpha)$ is generated by sampling independently from uniform distributions:

- Movement components $\Delta x, \Delta y \sim \mathcal{U}(-1, 1)$.
- The adherence level $\alpha \sim \mathcal{U}(0, 1)$.

This ensures that the agent explores the action space randomly without any directed objective, using the simulation's internal pseudo-random number generator for consistency.

C.5.3 Greedy Distance Maximizer Policy Implementation

The Greedy policy enacts a deterministic, reactive heuristic focused on maximizing immediate distance from the nearest identified threat. The implementation logic proceeds as follows at each timestep t:

1. **Identify Nearest Threat:** Let the agent's position at time t be $\mathbf{p}_a(t) = (x_a(t), y_a(t))$. Identify the set of currently infected humans $\mathcal{I}(t)$. This step utilizes privileged knowledge of the true state $S_j \in \{S, I, R, D\}$ for all humans j. If $\mathcal{I}(t)$ is empty, the agent defaults to a stationary action $\mathbf{m}^* = (0, 0)$.

2. **Target Selection:** If $\mathcal{I}(t)$ is not empty, calculate the Euclidean distance $d(\mathbf{p}_a(t), \mathbf{p}_j(t))$ for all $j \in \mathcal{I}(t)$, where $\mathbf{p}_j(t)$ is the position of infected human j and $d(\cdot, \cdot)$ accounts for the toroidal grid geometry. Identify the single infected human $h_{\text{nearest}}(t)$ corresponding to the minimum distance:

   $$h_{\text{nearest}}(t) = \arg\min_{j \in \mathcal{I}(t)} d(\mathbf{p}_a(t), \mathbf{p}_j(t))$$

   The exact position $\mathbf{p}_{h_{\text{nearest}}}(t)$ is **privileged information**.

3. **Evaluate Potential Moves:** Define a discrete set of candidate movement vectors $\mathcal{A}_{\text{move}}$. This set includes the zero vector $(0, 0)$ and scaled unit vectors representing the maximum possible step in the eight cardinal and diagonal directions, e.g., $\{(0, 0), (\pm s_M, 0), (0, \pm s_M), (\pm s_M/\sqrt{2}, \pm s_M/\sqrt{2})\}$, where s_M is the maximum movement scale (typically 1.0).

4. **Select Best Move:** For each candidate movement $\mathbf{m}_i = (\Delta x_i, \Delta y_i) \in \mathcal{A}_{\text{move}}$, calculate the agent's potential next position $\mathbf{p}'_{a,i}(t + 1)$ by applying the movement to $\mathbf{p}_a(t)$ and considering the grid's periodic boundaries. Evaluate the distance from this potential position to the initially identified nearest threat's current position $\mathbf{p}_{h_{\text{nearest}}}(t)$. Select the movement vector $\mathbf{m}^*$ that maximizes this distance:

   $$\mathbf{m}^* = \arg\max_{\mathbf{m}_i \in \mathcal{A}_{\text{move}}} d(\mathbf{p}'_{a,i}(t + 1), \mathbf{p}_{h_{\text{nearest}}}(t))$$

   This calculation relies on knowing $\mathbf{p}_{h_{\text{nearest}}}(t)$.

5. **Set Adherence:** The adherence component of the action is deterministically set to the maximum value, $\alpha = 1.0$.

6. **Final Action:** The resulting action for timestep t is $a(t) = (\mathbf{m}^*, \alpha = 1.0)$.

This implementation defines a simple, reactive strategy that exploits complete and accurate environmental state information to maximize instantaneous separation from the nearest perceived threat, while also employing maximum protective adherence.

D Results Continued

These figures and tables provide additional visualizations and experiments corresponding to those presented in the main Results section of the paper.

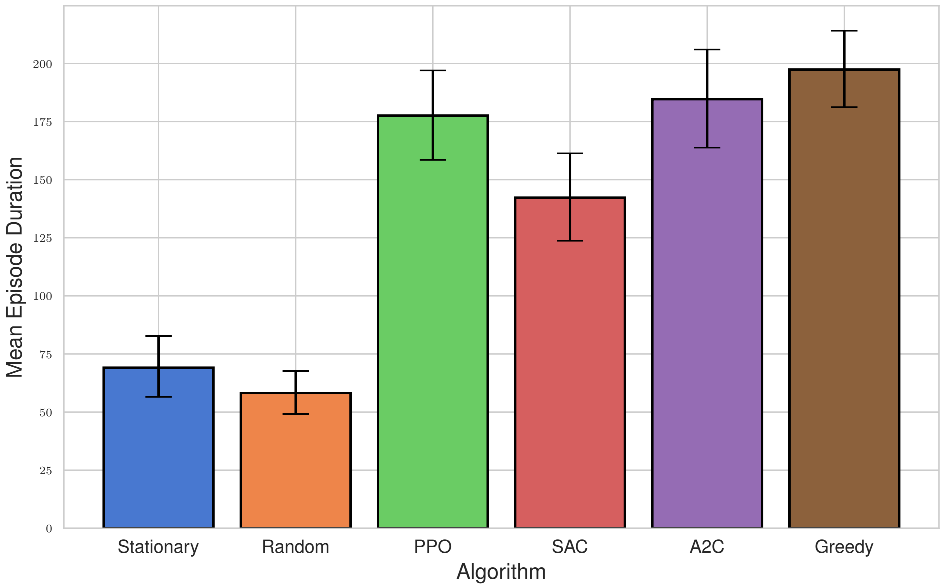

Figure 9: Mean episode durations and 95% bootstrapped confidence intervals (10,000 samples) for each agent. Values are aggregated across 3 training seeds and 100 evaluation episodes per seed. This figure summarizes the performance trends visualized in Figure 2.

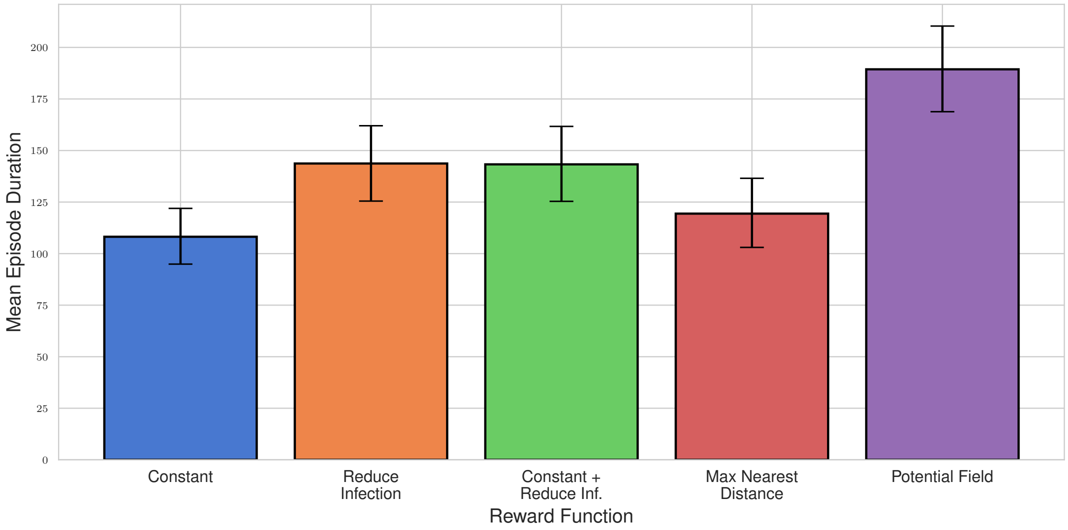

Figure 10: Mean episode durations with 95% bootstrapped confidence intervals (10,000 samples) for each reward function. These values correspond to the same experiments shown in Figure 3, aggregating performance across 3 seeds and 100 evaluations per seed.

Table 8: One-sided Mann–Whitney U test results comparing each reward function to the *Potential Field* baseline (PF). Bonferroni correction is applied to one-sided p-values. "Winner" denotes the reward function with significantly longer episode durations. Abbreviations: **Const** = Constant, **RedInfect** = Reduce Infection, **Combo** = Constant + Reduce Infection, **MaxDist** = Max Nearest Distance, **PF** = Potential Field. Significance: * $p < 0.05$, ** $p < 0.01$, *** $p < 0.001$, **n.s.** = not significant. This table supports the significance annotations shown in Figure 3.

Reward Function	**p (2-sided)**	**p (1-sided)**	**Sig (2)**	**Corrected p (1)**	**Sig (1)**	**Winner**
Const	3.38e-06	1.69e-06	***	6.76e-06	***	PF
RedInfect	0.00556	0.00278	**	0.0111	*	PF
Combo	0.00185	0.00092	**	0.00369	**	PF
MaxDist	1.04e-06	5.21e-07	***	2.08e-06	***	PF

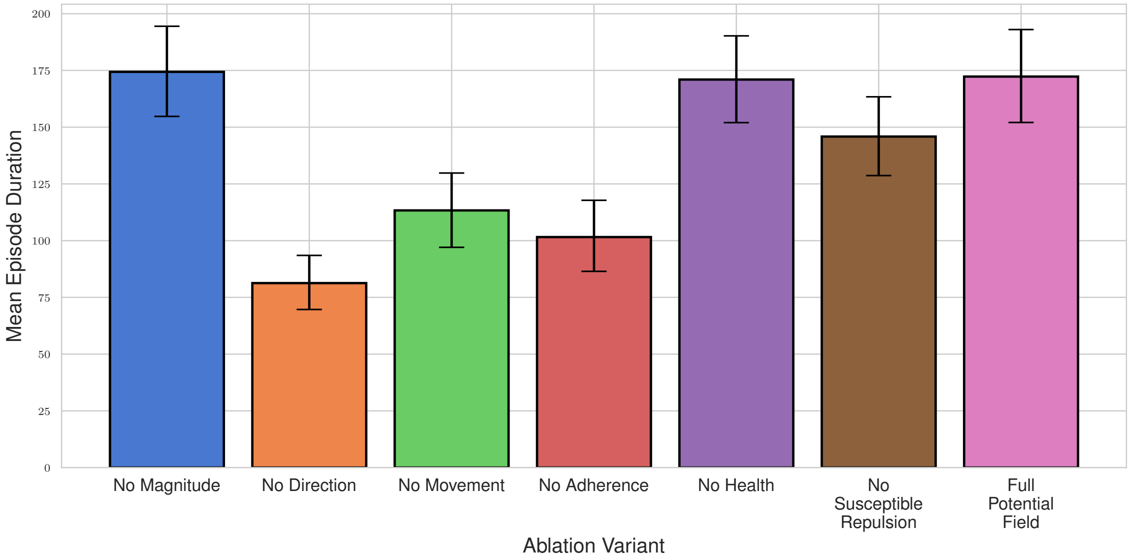

Figure 11: Mean episode durations and 95% bootstrapped confidence intervals (10,000 samples) for each ablation variant in the Potential Field reward study. These aggregate values summarize the same evaluations shown in Figure 4, providing a direct comparison of central performance tendencies across reward configurations.

Table 9: One-sided Mann–Whitney U test results comparing each ablation variant to the *Full Potential Field* (**FPF**), which represents the original, unmodified reward function. Bonferroni correction is applied to one-sided p-values. "Winner" indicates the variant with significantly longer episode durations. Significance levels: * $p < 0.05$, ** $p < 0.01$, *** $p < 0.001$, **n.s.** = not significant. Results support the differences shown in Figure 4.

Ablation Variant	**p (2-sided)**	**p (1-sided)**	**Sig (2)**	**p (1) Corr**	**Sig (1)**	**Winner**
No Magnitude	0.9571	0.5216	n.s.	1	n.s.	–
No Direction	3.80e-11	1.90e-11	***	1.14e-10	***	FPF
No Movement	6.93e-06	3.46e-06	***	2.08e-05	***	FPF
No Adherence	3.88e-09	1.94e-09	***	1.16e-08	***	FPF
No Health	0.8242	0.5881	n.s.	1	n.s.	–
No Susceptible Repulsion	0.1336	0.0668	n.s.	0.4007	n.s.	–

Table 10: Statistical significance tests comparing RL agents trained with different visibility radius constraints in epidemic control. Agents were trained and evaluated with Full Visibility, Limited Visibility r=10, r=15, and r=20 (where r represents the radius within which the agent can observe infected individuals). Each condition used 300 episodes (3 seeds × 100 episodes per seed). Statistical significance determined using Mann-Whitney U tests with Bonferroni correction for 18 multiple comparisons (corrected $\alpha = 0.002778$). Tests compare trained agents against baselines (Stationary, Random, Greedy) and trained agents against each other to assess the impact of visibility constraints on performance.

Category	**Comparison**	**Winner**	**U-stat.**	**p-value**	**Sig.**
Trained vs Baselines	Full vs Stationary	Full	79,732.0	$p < 0.001$	***
	Full vs Random	Full	66,639.0	$p < 0.001$	***
	Full vs Greedy	Full	46,927.0	$p = 1.000$	n.s.
	r=10 vs Stationary	r=10	82,063.0	$p < 0.001$	***
	r=10 vs Random	r=10	73,277.0	$p < 0.001$	***
	r=10 vs Greedy	r=10	55,948.0	$p < 0.001$	***
	r=15 vs Stationary	r=15	83,000.0	$p < 0.001$	***
	r=15 vs Random	r=15	74,393.0	$p < 0.001$	***
	r=15 vs Greedy	r=15	59,913.0	$p < 0.001$	***
	r=20 vs Stationary	r=20	82,436.0	$p < 0.001$	***
	r=20 vs Random	r=20	72,773.0	$p < 0.001$	***
	r=20 vs Greedy	r=20	57,229.0	$p < 0.001$	***
Trained vs Trained	Full vs r=10	r=10	35,009.0	$p < 0.001$	***
	Full vs r=15	r=15	31,504.0	$p < 0.001$	***
	Full vs r=20	r=20	34,320.0	$p < 0.001$	***
	r=10 vs r=15	r=15	40,943.0	$p = 1.000$	n.s.
	r=10 vs r=20	r=20	43,770.0	$p = 1.000$	n.s.
	r=15 vs r=20	r=15	47,696.0	$p = 1.000$	n.s.

Table 11: Results of two-sided and one-sided Mann–Whitney U tests comparing **Trained** agents to baselines (**Stationary**, **Random**, **Greedy**) across four infection rates (β). Each comparison uses 300 evaluation episodes (100 per seed over 3 seeds). The one-sided p-values are Bonferroni-corrected within each β group. "Winner" indicates the agent with significantly longer episode durations based on the corrected one-sided test. Significance levels: * $p < 0.05$, ** $p < 0.01$, *** $p < 0.001$, **n.s.** = not significant.

β	Baseline	p (2-sided)	p (1-sided)	Sig (2)	p (1) Corr	Sig (1)	Winner
0.2	Stationary	2.86×10^{-17}	1.43×10^{-17}	***	4.30×10^{-17}	***	Trained
	Random	6.87×10^{-24}	3.43×10^{-24}	***	1.03×10^{-23}	***	Trained
	Greedy	2.03×10^{-21}	1.02×10^{-21}	***	3.05×10^{-21}	***	Greedy
0.5	Stationary	1.01×10^{-16}	5.06×10^{-17}	***	1.52×10^{-16}	***	Trained
	Random	5.13×10^{-15}	2.57×10^{-15}	***	7.70×10^{-15}	***	Trained
	Greedy	1.29×10^{-46}	6.45×10^{-47}	***	1.94×10^{-46}	***	Greedy
0.7	Stationary	9.82×10^{-16}	4.91×10^{-16}	***	1.47×10^{-15}	***	Trained
	Random	2.37×10^{-12}	1.18×10^{-12}	***	3.55×10^{-12}	***	Trained
	Greedy	1.56×10^{-27}	7.79×10^{-28}	***	2.34×10^{-27}	***	Greedy
0.9	Stationary	5.46×10^{-27}	2.73×10^{-27}	***	8.19×10^{-27}	***	Trained
	Random	2.53×10^{-15}	1.27×10^{-15}	***	3.80×10^{-15}	***	Trained
	Greedy	6.74×10^{-23}	3.37×10^{-23}	***	1.01×10^{-22}	***	Greedy

E Compute Resources

All experiments were conducted on Apple Silicon M4 chip workers (16-core CPU) with 48 GB LPDDR5 unified memory. We devoted approximately 40 CPU-hours to hyperparameter optimization. All training and evaluation were performed across 3 random seeds (with 100 runs per seed unless otherwise specified). Training times for each set of experiments were approximately as follows:

- Comparison of different RL algorithms: 22 hours
- Ablation studies of the potential field reward function: 13 hours
- Comparison of reward functions: 14 hours
- Comparison of POMDP and full observability (MDP): 15 hours
- Constraints in Movement: 12 hours
- Additional results and experiments (in appendix): 26 hours

F Additional Results and Experiments

In the supplementary experiments presented here, we vary one environmental parameter of the epidemic at a time to simulate a range of spatial epidemic scenarios constructible with ContagionRL. This allows us to explore both favorable and challenging conditions under which to stress-test agent learning. For each experiment, we provide two outputs: a grouped bar plot illustrating mean episode durations with 95% confidence intervals, and a table reporting results from one-sided and two-sided Mann–Whitney U tests. All experiments in this section use PPO for training, with hyperparameters defined in Appendix C.4 and environment configurations in Appendix C.2. Each table and figure corresponds to a single modified environmental parameter specified in their respective captions.

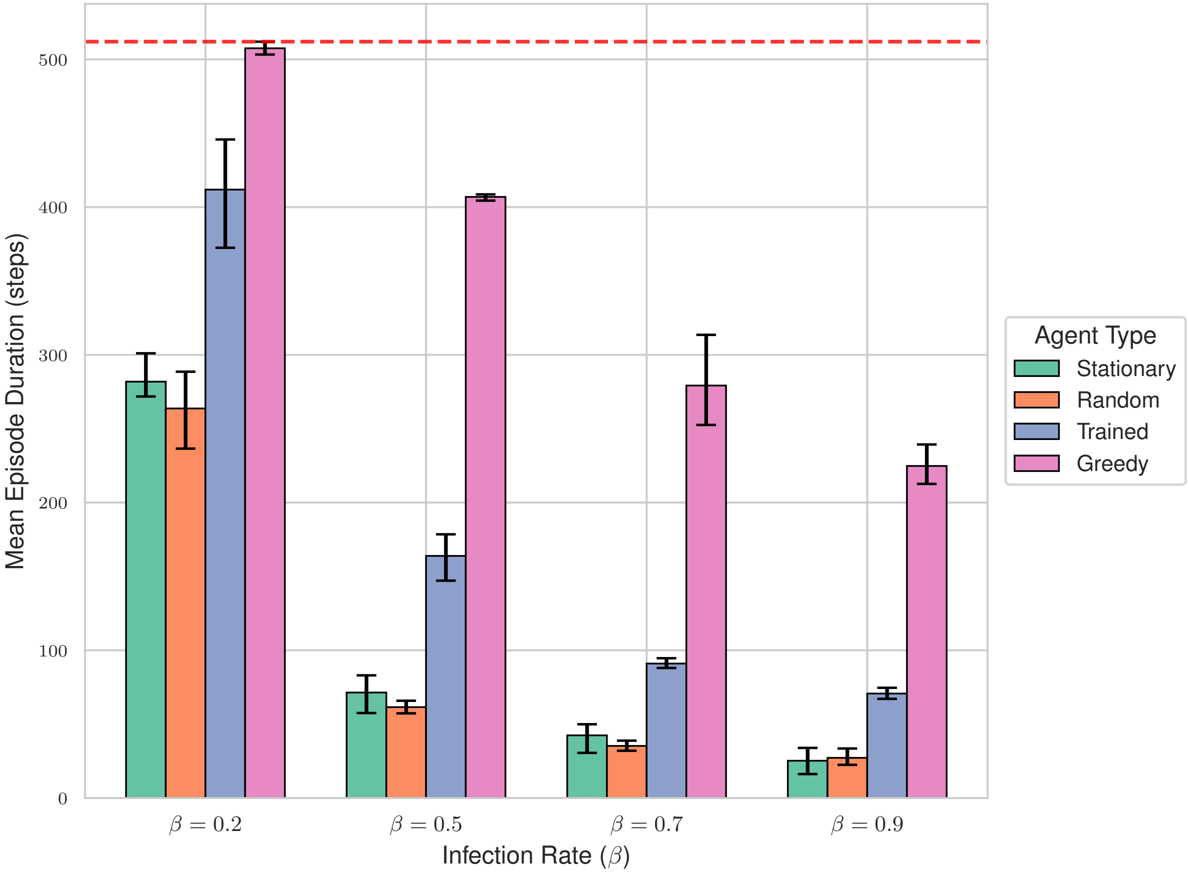

Figure 12: Comparison of mean episode durations across agents (Trained, Stationary, Random, Greedy) for different infection rates β. Bars indicate the mean episode duration over 3 seeds (each evaluated for 100 episodes, totaling 300 episodes per agent), with 95% bootstrapped confidence intervals (10,000 resamples). The dashed red line marks the maximum possible episode duration. See Table 11 for detailed two-sided and one-sided Mann–Whitney U test results with Bonferroni correction.

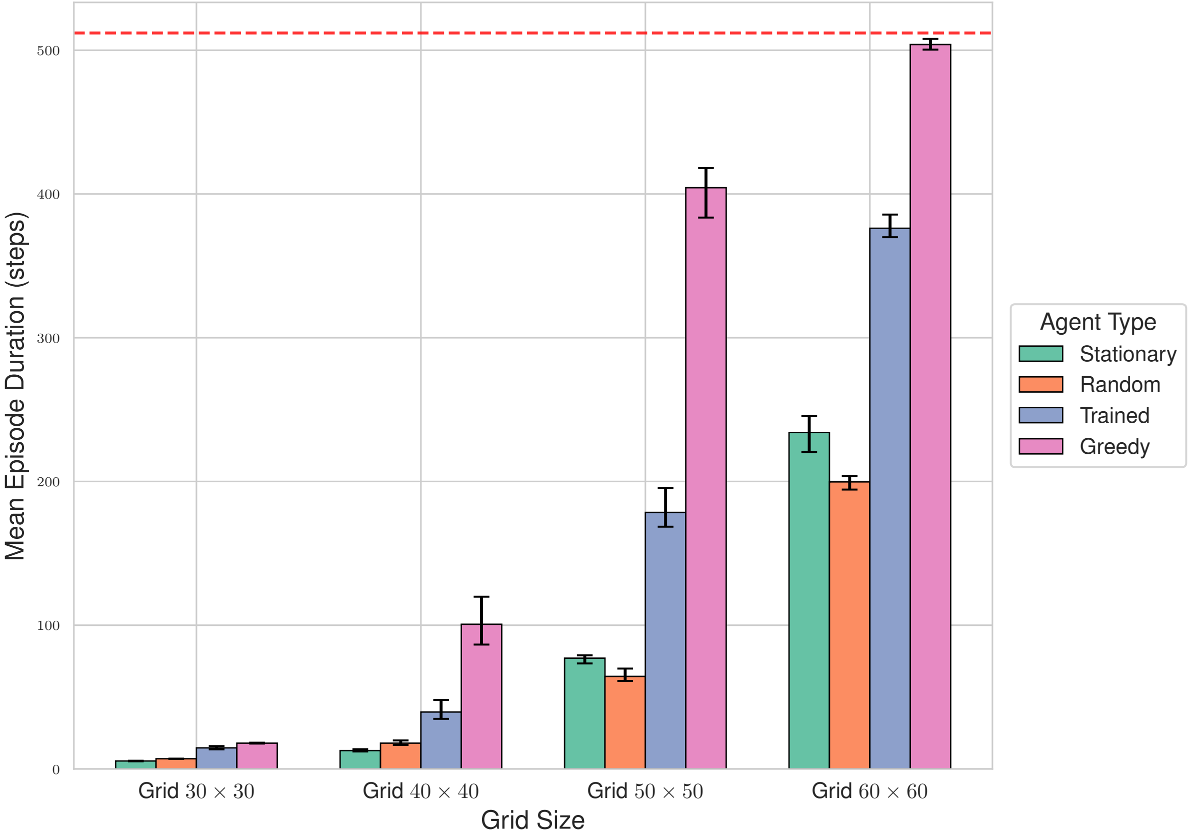

Figure 13: Mean episode durations for *Trained*, *Stationary*, *Random*, and *Greedy* agents evaluated across environments with varying grid sizes. Each bar represents the mean across 3 seeds (each with 100 evaluation episodes), and is accompanied by 95% bootstrapped confidence intervals (10,000 resamples). The red dashed line marks the maximum episode length. See Table 12 for statistical comparisons between *Trained* and baseline agents using both one-sided and two-sided Mann–Whitney U tests with Bonferroni correction.

Table 12: One-sided and two-sided Mann–Whitney U test results comparing *Trained* agents to baseline agents across varying grid sizes. For each grid configuration, we tested whether the *Trained* agent achieves significantly longer episode durations than *Stationary*, *Random*, and *Greedy* baselines. Bonferroni correction is applied to the one-sided p-values. Significance levels: * $p < 0.05$, ** $p < 0.01$, *** $p < 0.001$, **n.s.** = not significant. "Winner" indicates the model with significantly longer duration after correction. "Mean Diff" refers to (Trained − Baseline) mean.

Grid	Baseline	p (2-sid.)	p (1-sid.)	Sig (2)	p (1) Corr	Sig (1)	Winner	Mean Diff
30 × 30	Stationary	1.96e-40	9.80e-41	***	2.94e-40	***	Trained	9.12
	Random	1.62e-24	8.13e-25	***	2.44e-24	***	Trained	7.56
	Greedy	0.1482	0.0741	n.s.	0.2223	n.s.	–	−3.27
40 × 40	Stationary	3.11e-29	1.55e-29	***	4.67e-29	***	Trained	26.81
	Random	1.74e-17	8.71e-18	***	2.61e-17	***	Trained	21.66
	Greedy	6.47e-12	3.23e-12	***	9.70e-12	***	Greedy	−61.05
50 × 50	Stationary	1.01e-16	5.06e-17	***	1.52e-16	***	Trained	101.40
	Random	4.04e-16	2.02e-16	***	6.06e-16	***	Trained	114.08
	Greedy	2.07e-37	1.04e-37	***	3.11e-37	***	Greedy	−225.88
60 × 60	Stationary	7.98e-16	3.99e-16	***	1.20e-15	***	Trained	142.10
	Random	4.25e-24	2.13e-24	***	6.38e-24	***	Trained	176.46
	Greedy	1.12e-24	5.57e-25	***	1.67e-24	***	Greedy	−127.80

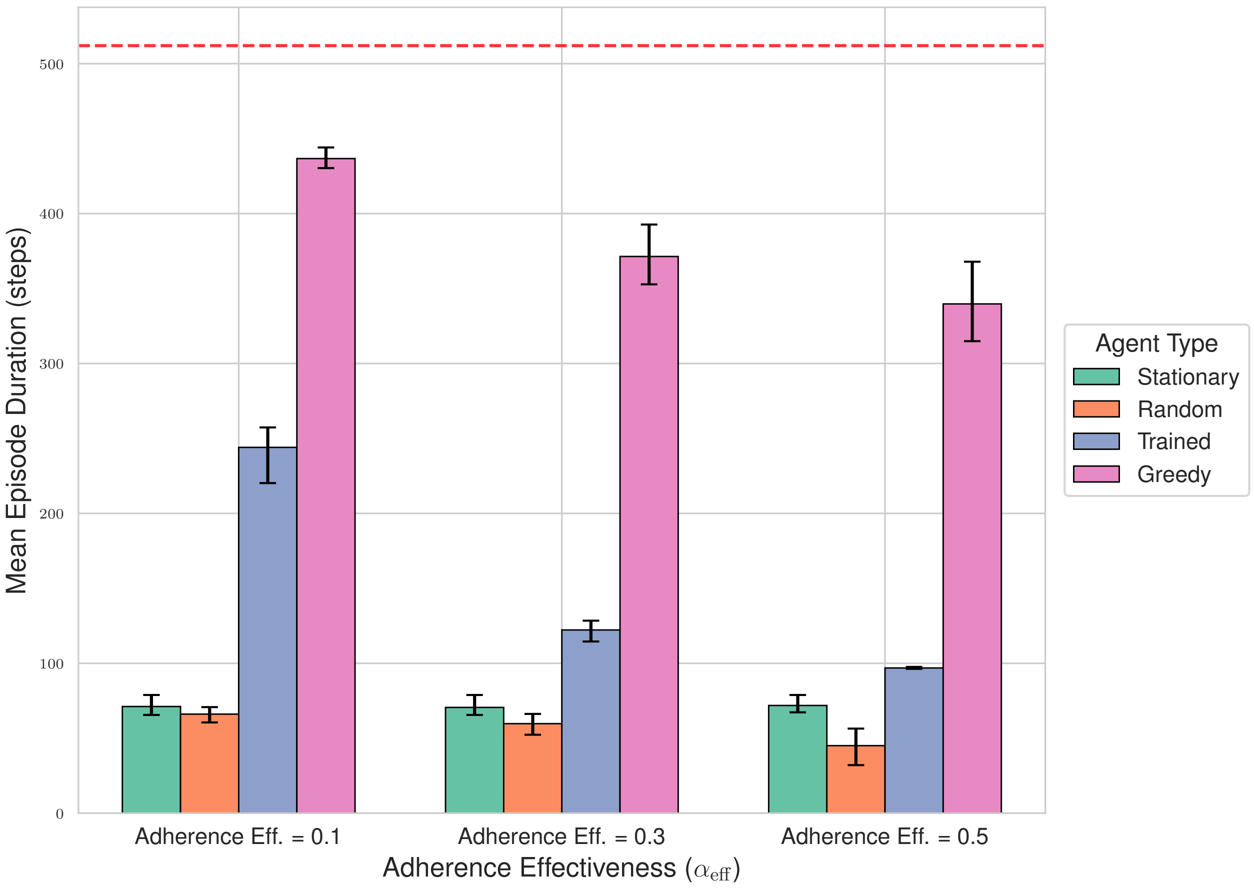

Figure 14: Mean episode durations of *Trained*, *Stationary*, *Random*, and *Greedy* agents across varying levels of adherence effectiveness. Each bar represents the mean of 3 independent training runs, each evaluated over 100 episodes (300 evaluations per agent-type per setting), with 95% bootstrapped confidence intervals (10,000 resamples). A red dashed line indicates the maximum episode length imposed by the environment. Statistical comparisons between the *Trained* agent and each baseline are provided in Table 13, using one-sided and two-sided Mann–Whitney U tests with Bonferroni correction.

Table 13: Mann–Whitney U test results comparing *Trained* agents to *Stationary*, *Random*, and *Greedy* baselines under varying adherence effectiveness. Both two-sided and one-sided tests were performed. One-sided p-values were Bonferroni-corrected. "Winner" indicates the agent with significantly longer episode duration. "Mean Diff" is Trained minus Baseline. Significance: * $p < 0.05$, ** $p < 0.01$, *** $p < 0.001$, **n.s.** = not significant.

Adh. Eff.	Baseline	p (2-sid.)	p (1-sid.)	Sig (2)	p (1) Corr	Sig (1)	Winner	Mean Diff
0.1	Stationary	1.05e-35	5.25e-36	***	1.58e-35	***	Trained	172.85
	Random	4.14e-33	2.07e-33	***	6.21e-33	***	Trained	177.92
	Greedy	4.49e-34	2.24e-34	***	6.73e-34	***	Greedy	−192.65
0.3	Stationary	1.07e-08	5.37e-09	***	1.61e-08	***	Trained	51.67
	Random	2.36e-06	1.18e-06	***	3.55e-06	***	Trained	62.49
	Greedy	1.22e-43	6.12e-44	***	1.84e-43	***	Greedy	−249.12
0.5	Stationary	0.0180	0.0090	*	0.0270	*	Trained	25.03
	Random	6.83e-06	3.42e-06	***	1.03e-05	***	Trained	51.82
	Greedy	4.72e-42	2.36e-42	***	7.07e-42	***	Greedy	−242.83

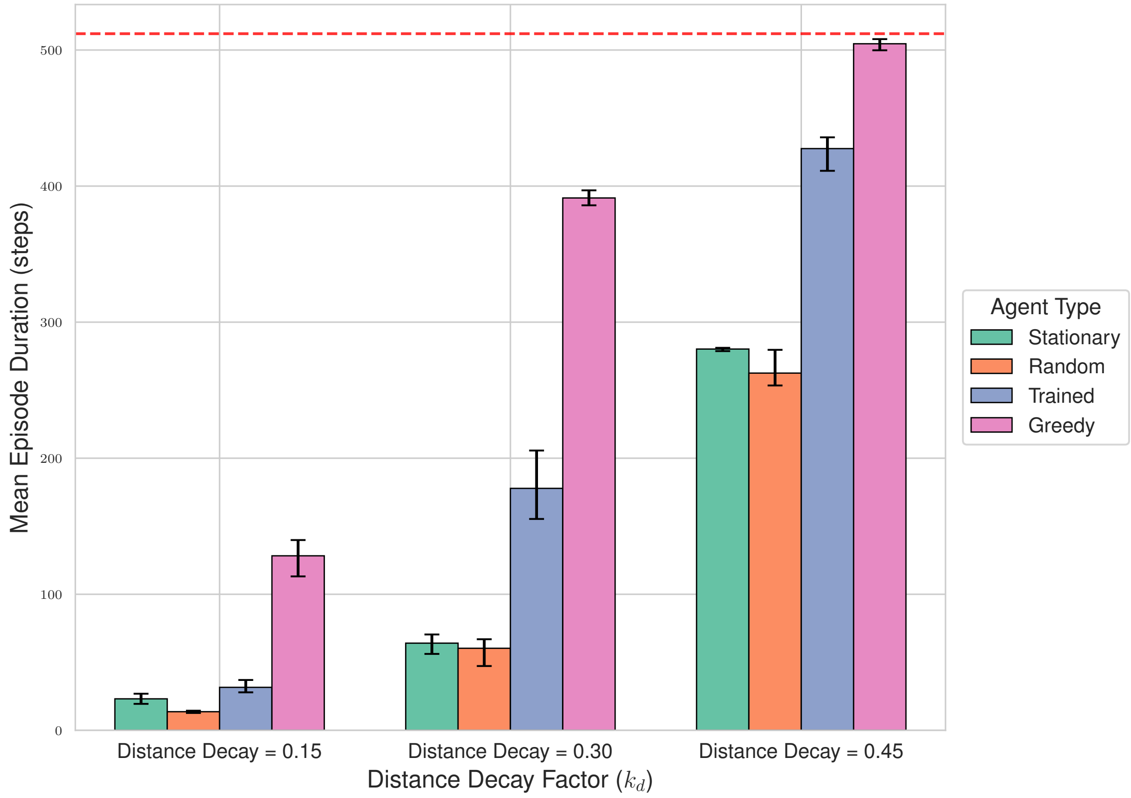

Figure 15: Performance comparison of *Trained* and baseline agents across varying values of the *distance decay* parameter, which controls how repulsion from infected individuals diminishes with spatial separation. Bars show mean episode durations, with 95% bootstrapped confidence intervals (10,000 samples) calculated from per-seed means. The red dashed line indicates the maximum episode duration. For a statistical analysis of whether *Trained* agents significantly outperform baselines, see Table 14.

Table 14: Mann–Whitney U test results comparing *Trained* agents to *Stationary*, *Random*, and *Greedy* baselines across varying levels of the *distance decay* parameter. Both two-sided and one-sided tests were performed. One-sided p-values were corrected using Bonferroni correction. "Winner" denotes the agent with significantly longer episode durations after correction. "Mean Diff" reports the difference in mean episode duration between *Trained* and baseline (positive = *Trained* better). Significance thresholds: * $p < 0.05$, ** $p < 0.01$, *** $p < 0.001$, **n.s.** = not significant.

Dist. Decay	Baseline	p (2-sid.)	p (1-sid.)	Sig (2)	p (1) Corr	Sig (1)	Winner	Mean Diff
0.15	Stationary	2.42e-26	1.21e-26	***	3.63e-26	***	Trained	8.44
	Random	3.97e-18	1.99e-18	***	5.96e-18	***	Trained	17.90
	Greedy	6.77e-14	3.39e-14	***	1.02e-13	***	Greedy	−96.67
0.30	Stationary	1.09e-24	5.44e-25	***	1.63e-24	***	Trained	113.78
	Random	1.73e-21	8.64e-22	***	2.59e-21	***	Trained	117.54
	Greedy	9.73e-35	4.86e-35	***	1.46e-34	***	Greedy	−213.42
0.45	Stationary	2.91e-21	1.46e-21	***	4.37e-21	***	Trained	147.33
	Random	2.84e-28	1.42e-28	***	4.26e-28	***	Trained	165.01
	Greedy	1.42e-15	7.11e-16	***	2.13e-15	***	Greedy	−77.05